

Imperfect molecular detection renormalizes apparent kinetic rates in stochastic gene regulatory networks

Iryna Zabaikina¹ and Ramon Grima^{*2}

¹*Department of Mathematical Analysis and Numerical Mathematics, Comenius Univ., Slovakia*

³*School of Biological Sciences, University of Edinburgh, UK*

Abstract

Imperfect molecular detection in single-cell experiments introduces technical noise that obscures the true stochastic dynamics of gene regulatory networks. While binomial models of molecular capture provide a principled description of imperfect detection, they have so far been analyzed only for simple gene-expression models that do not explicitly account for regulation. Here, we extend binomial models of capture to general gene regulatory networks to understand how imperfect capture reshapes the observed time-dependent statistics of molecular counts. Our results reveal when capture effects correspond to a renormalization of a subset of the kinetic rates and when they cannot be absorbed into effective rates, providing a systematic basis for interpreting noisy single-cell measurements. In particular, we show that rate renormalization emerges either under significant transcription factor abundance or when promoter-state transitions occur on a distinct (much slower or faster) timescale than other reactions. In these cases, technical noise causes the apparent mean burst size of synthesized gene products to appear reduced while transcription factor binding reactions appear faster. These effects hold for gene regulatory networks of arbitrary connectivity and remain valid under time-dependent kinetic rates.

1 Introduction

Understanding the dynamics of gene regulatory networks (GRNs) is a central goal of systems biology because they play an important role in every process of life, including cell differentiation, metabolism, the cell cycle and signal transduction [1, 2, 3]. Gene expression is inherently noisy [4], and hence, mathematical models are widely used to characterize fluctuations in mRNA and protein numbers and to link these fluctuations to underlying regulatory mechanisms [5, 6, 7, 8, 9, 10, 11, 12, 13, 14]. However, virtually all existing stochastic models make an implicit strong assumption: that measurements of molecule numbers inside cells are perfect, meaning that every molecule present is detected in the experimental readout and that technical noise is absent.

Using modern single-cell technologies, only a fraction of the molecules in each cell are actually captured and observed. This disconnect between the underlying biochemical dynamics and the measurement process motivates the need for explicit measurement models that augment stochastic models of the dynamics of GRNs.

Two classes of measurement models are commonly used. The first is *zero-inflation*, where the observed distribution is modeled as a mixture between a point mass at zero and the expression distribution generated by an underlying gene-expression model. The aim is to capture the increase in the artificial number of zeros due to imperfect molecular detection. Zero-inflated models have been widely used to analyze single-cell RNA sequencing (scRNA-seq) data [15, 16, 17, 18], and attempts have been made to justify zero-inflation mechanistically [19]. However, zero-inflation is not ideal. Clearly, downsampling due to imperfect capture increases not only the number of zeros but also changes the number of all non-zero counts.

A more principled and increasingly preferred alternative is the *binomial capture model* [20]. In this model, each molecule is independently captured and detected with probability p (Fig. 1). Given n actual molecules, the number of detected molecules is then a random variable distributed according to the binomial distribution with number of trials n and probability p . This model has been shown to be consistent with the statistics of raw experimental scRNA-seq data [21] and it is indeed a reasonable simple model for the detection of any type of molecule. Empirical studies estimate typical capture probabilities for mRNA between 0.05 and 0.3, depending on the single-cell sequencing platform [22, 23, 24, 25]. State-of-the-art single-cell proteomics can detect thousands of proteins per cell [26, 27], but the effective per-protein capture efficiency is poorly quantified and current values are

*Correspondence: ramon.grima@ed.ac.uk

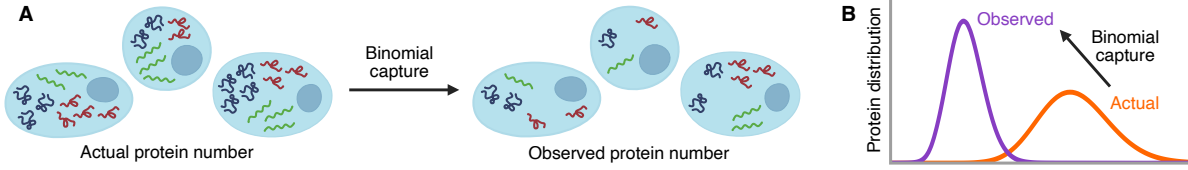


Figure 1: Illustration of the binomial model of molecular capture. In an experiment, only a fraction p of the original molecular counts are detected. This leads to a distribution of observed counts that is a downsampled version of the actual distribution of counts.

only rough estimates, with abundant proteins detected in tens of percent of cells and low-copy proteins much less frequently — in fact, over 75% missing values is the rule for single-cell proteomics data sets [28].

Thus far, binomial capture models have been studied mainly in the context of simple gene-expression models [29, 30, 31, 32], which only predict mRNA distributions and do not include explicit regulatory reactions such as transcription factor-promoter interactions. For the telegraph model [33] in steady-state conditions, the effect of binomial capture leads to a simple rescaling of the mRNA synthesis rate by a factor p (the capture probability). Consequently, it remains unclear whether, and in what form, binomial capture induces a renormalization of reaction rates when incorporated as a measurement model for GRN dynamics, including the case of time-dependent kinetic rates.

In this paper, we extend binomial capture models to general GRNs and investigate how technical noise affects the *observed* stochastic dynamics of regulated gene expression. This framework allows us to determine how imperfect capture distorts distributions of molecular counts and to identify when the effects of technical noise can be absorbed into effective rate parameters of the underlying gene-regulatory model. The paper is divided into two main parts. In Section 2, we investigate the impact of technical noise using a discrete chemical master approach and study in detail the common motif of an auto-regulatory gene. In Section 3, we investigate the impact of technical noise using a piecewise-deterministic approach and derive results for general gene regulatory networks composed of an arbitrary number of interacting genes. We conclude by a discussion in Section 4.

2 Count distribution prediction under technical noise using a discrete approach

2.1 The Binomial Capture Model

Let the probability of detecting a molecule of a particular type in a cell be p and the actual number of molecules of this type to be y . As stated earlier, it follows that the number of measured molecules x is a random variable sampled from the binomial distribution with number of trials y , number of successes x and probability of success p . Assuming each cell has the same capture probability p , the distribution of the observed molecular counts $P(x)$ is given by

$$P(x) = \sum_{y=0}^{\infty} P_{\text{bin}}^p(x|y)Q(y), \quad (1)$$

where $Q(y)$ is the distribution of true counts and $P_{\text{bin}}^p(x|y)$ is the binomial distribution

$$P_{\text{bin}}^p(x|y) = \binom{y}{x} p^x (1-p)^{y-x}. \quad (2)$$

It immediately follows that for any integer r , the r -th factorial moment of the distribution of the observed counts can be written in terms of the r -th factorial moment of the distribution of the true counts:

$$\langle (x)_r \rangle = \langle x(x-1)\dots(x-r+1) \rangle = \sum_x (x)_r P(x) = p^r \langle (y)_r \rangle, \quad (3)$$

where $\langle (y)_r \rangle = \sum_y y(y-1)\dots(y-r+1)Q(y)$. Note that here we used the identity:

$$\sum_x (x)_r P_{\text{bin}}^p(y, x) = p^r (y)_r. \quad (4)$$

From this formula, we can construct equations for various statistical quantities of interest such as the mean and the variance of the observed counts in terms of those of the actual counts:

$$\langle x \rangle = p \langle y \rangle, \quad (5)$$

$$\sigma_x^2 = \langle x \rangle \left[1 + p \left(\frac{\sigma_y^2}{\langle y \rangle} - 1 \right) \right]. \quad (6)$$

The multivariate extension of Eq. (1) is straightforward:

$$P(x_1, \dots, x_R) = \sum_{y_1=0, \dots, y_R=0}^{\infty} P_{\text{bin}}^{p_1}(x_1|y_1) \dots P_{\text{bin}}^{p_R}(x_R|y_R) Q(y_1, \dots, y_R), \quad (7)$$

where $P(x_1, \dots, x_R)$ is the joint distribution of observed counts, $Q(y_1, \dots, y_R)$ is the joint distribution of true counts and p_i is the capture probability for the i -th species.

2.1.1 Technical noise in generating function space

Using Eq. (7), the generating function of the distribution of observed counts is given by

$$\begin{aligned} G(z_1, \dots, z_R, t) &= \sum_{x_1=0}^{\infty} \dots \sum_{x_R=0}^{\infty} z_1^{x_1} \dots z_R^{x_R} P(x_1, \dots, x_R, t) \\ &= \sum_{y_1=0}^{\infty} \dots \sum_{y_R=0}^{\infty} (1 - p_1(1 - z_1))^{y_1} \dots (1 - p_R(1 - z_R))^{y_R} Q(y_1, \dots, y_R, t). \end{aligned} \quad (8)$$

By contrast, the generating function of the distribution of the true counts is given by

$$G(z_1, \dots, z_R, t)^* = \sum_{y_1=0}^{\infty} \dots \sum_{y_R=0}^{\infty} z_1^{y_1} \dots z_R^{y_R} Q(y_1, \dots, y_R, t). \quad (9)$$

Comparing the two generating functions, we see that the generating function of the distribution of observed counts can be directly obtained from the generating function of the distribution of the true counts by replacing z_i in the latter expression by $1 - p_i(1 - z_i)$.

2.2 The influence of technical noise on models without any explicit regulatory dynamics

In this section, we explore models of stochastic gene expression where regulatory effects are captured implicitly through promoter state transitions, rather than through a detailed representation of transcription factor binding.

2.2.1 Telegraph model of gene expression with time-dependent rates



This is the telegraph model of gene expression from a single gene copy where D_{on} is the promoter in the active state, D_{off} is the promoter in the inactive state and M is mRNA [33, 34]. The promoter can switch between active and inactive states, mRNA is transcribed when the promoter is active, and subsequently it decays. The only difference from the original telegraph model is that we consider all kinetic rates to be time-dependent.

We consider only the mRNA to be observable, the typical experimental scenario, when using single-molecule fluorescent in situ hybridization (smFISH) or scRNA-seq. We first write the chemical master equations for the

probability of observing mRNA conditioned on the promoter states:

$$\begin{aligned} \frac{\partial Q_{\text{on}}(m, t)}{\partial t} &= k_3(t)(Q_{\text{on}}(m-1, t) - Q_{\text{on}}(m, t)) + k_4(t)((m+1)Q_{\text{on}}(m+1, t) - mQ_{\text{on}}(m, t)) \\ &\quad - k_1(t)Q_{\text{on}}(m, t) + k_2(t)Q_{\text{off}}(m, t), \end{aligned} \quad (11)$$

$$\frac{\partial Q_{\text{off}}(m, t)}{\partial t} = k_4(t)((m+1)Q_{\text{off}}(m+1, t) - mQ_{\text{off}}(m, t)) + k_1(t)Q_{\text{on}}(m, t) - k_2(t)Q_{\text{off}}(m, t), \quad (12)$$

where $Q_{\text{on}}(m, t)$ is the probability of observing m mRNA molecules at time t when the promoter is on and $Q_{\text{off}}(m, t)$ is the probability of observing m mRNA molecules at time t when the promoter is off.

The generating function equations corresponding to these conditional master equations are

$$\begin{aligned} \frac{\partial G_{\text{on}}^*(z, t)}{\partial t} &= k_3(t)(z-1)G_{\text{on}}^*(z, t) - k_4(t)(z-1)\frac{\partial G_{\text{on}}^*(z, t)}{\partial z} - k_1(t)G_{\text{on}}^*(z, t) + k_2(t)G_{\text{off}}^*(z, t), \\ \frac{\partial G_{\text{off}}^*(z, t)}{\partial t} &= -k_4(t)(z-1)\frac{\partial G_{\text{off}}^*(z, t)}{\partial z} + k_1(t)G_{\text{on}}^*(z, t) - k_2(t)G_{\text{off}}^*(z, t), \end{aligned} \quad (13)$$

with initial conditions $G_{\text{off}}^*(z, 0) = f_0(z)$ and $G_{\text{on}}^*(z, 0) = f_1(z)$.

According to the results of Section 2.1.1, the generating functions of the observed mRNA counts are found by replacing z by $1 - p(1 - z)$ and replacing G^* by G :

$$\begin{aligned} \frac{\partial G_{\text{on}}(z, t)}{\partial t} &= pk_3(t)(z-1)G_{\text{on}}(z, t) - k_4(t)(z-1)\frac{\partial G_{\text{on}}(z, t)}{\partial z} - k_1(t)G_{\text{on}}(z, t) + k_2(t)G_{\text{off}}(z, t), \\ \frac{\partial G_{\text{off}}(z, t)}{\partial t} &= -k_4(t)(z-1)\frac{\partial G_{\text{off}}(z, t)}{\partial z} + k_1(t)G_{\text{on}}(z, t) - k_2(t)G_{\text{off}}(z, t), \end{aligned} \quad (14)$$

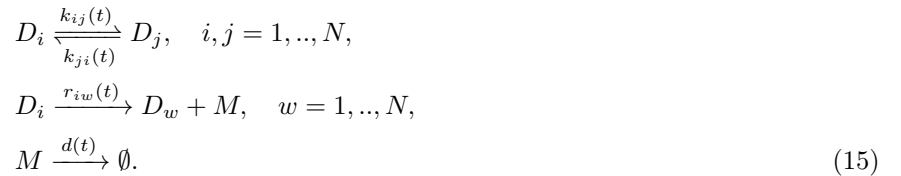
with initial conditions $G_{\text{off}}(z, 0) = f_0(1 - p(1 - z))$ and $G_{\text{on}}(z, 0) = f_1(1 - p(1 - z))$.

Note the generating function of the marginal mRNA distribution is $G(z, t) = G_{\text{on}}(z, t) + G_{\text{off}}(z, t)$. From a comparison of Eqs. (13) and (14) it follows that for all times the dynamics of the observed mRNA are exactly equivalent to those of the true system with appropriately chosen initial conditions and a renormalized transcription rate: $k_3(t) \mapsto pk_3(t)$.

Note that this result is already known for the special case where all rates are time-independent constants and assuming steady-state conditions [29, 31]; in this case, it trivially follows from the fact that the mRNA counts of the original telegraph model are distributed according to a Beta-Poisson distribution. Our simple derivation generalizes this to the case of time-dependent rates and non-steady-state conditions, and the derivation avoids any explicit solution of the chemical master equation.

2.2.2 Multi-state model of gene expression with time-dependent rates

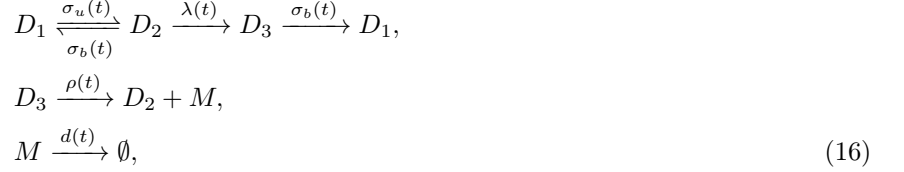
Next, we consider a more general version of the telegraph model where a promoter can be in N states, transitions between all states are allowed, and mRNA is produced from any promoter state, potentially also leading to a different promoter state upon production, e.g. modeling the clearing of the promoter for the next round of initiation after productive RNAP elongation starts [35, 36, 37, 38]. The reaction scheme for this system is given by



Several commonly used multi-state models [39, 40, 41, 42, 43] including a detailed ten-state initiation process based on a canonical model of eukaryotic transcription initiation [35] are special cases of this model.

Following the same approach as for the telegraph model in Section 2.2.1, we can write the generating functions of the true mRNA conditioned on the promoter state. Upon the change of variable z to $1 - p(1 - z)$, we find that for all times the generating function equations of the observed mRNA are the same as that of the true one with the transcription rates renormalized from $r_{iw}(t)$ to $pr_{iw}(t)$, provided $i = w$, i.e. if the promoter state does not change when transcription occurs.

However, if $i \neq w$ then this is not generally the case. For example, consider the three-state system studied in [44, 37] which is described by the reaction scheme



whereby a gene fluctuates between three states: two permissive states (D_2 and D_3) and a non-permissive state (D_1). The reactions effectively model the following processes. The transition from D_1 to D_2 (burst initiation) occurs through reversible transcription factor binding. Polymerase then binds to D_2 , producing the paused state D_3 , consistent with observations that polymerase pauses downstream of the initiation site before elongation (proximal-promoter pausing, a common feature of promoters in mammals and *Drosophila melanogaster* [45]). Release of polymerase from D_3 triggers two events: production of nascent mRNA (M) and a return of the gene to D_2 , reflecting that new polymerase cannot bind until the previous one unpauses [46]. In the paused state D_3 , both polymerase and the transcription factor may dissociate, returning the gene to the non-permissive state D_1 (burst termination).

The generating function equations for this system are given by

$$\begin{aligned} \frac{\partial G_1^*(z, t)}{\partial t} &= -d(t)(z-1) \frac{\partial G_1^*(z, t)}{\partial z} - \sigma_u(t)(t)G_1^*(z, t) + \sigma_b(t)(G_2^*(z, t) + G_3^*(z, t)), \\ \frac{\partial G_2^*(z, t)}{\partial t} &= -d(t)(z-1) \frac{\partial G_2^*(z, t)}{\partial z} + \rho(t)zG_3^*(z, t) - (\sigma_b(t) + \lambda(t))G_2^*(z, t) + \sigma_u(t)G_1^*(z, t), \\ \frac{\partial G_3^*(z, t)}{\partial t} &= -d(t)(z-1) \frac{\partial G_3^*(z, t)}{\partial z} - \rho(t)G_3^*(z, t) - \sigma_b(t)G_3^*(z, t) + \lambda G_2^*(z, t). \end{aligned} \quad (17)$$

Upon the change of variable z to $1 - p(1 - z)$, we find that the generating function equations of the observed mRNA are not the same as that of the true one with renormalized rates. The reason is that the term $\rho(t)zG_3^*(z, t)$ in the second equation does not transform to $\rho(t)pzG_3^*(z, t)$ but to $\rho(t)(1 - p(1 - z))G_3^*(z, t)$. The same can also be deduced by examining the exact steady-state solution of Eq. (17) when the rates are time-independent constants [37]:

$$G^*(z) = G_1^*(z) + G_2^*(z) + G_3^*(z) = {}_1F_2\left(\frac{\sigma_u}{d}; \frac{\sigma_u + \sigma_b}{d}, \frac{\sigma_b + \rho + \lambda}{d}; \frac{\rho\lambda}{d^2}(z-1)\right), \quad (18)$$

which implies that the generating function of observed mRNA is

$$G(z) = G_1(z) + G_2(z) + G_3(z) = {}_1F_2\left(\frac{\sigma_u}{d}; \frac{\sigma_u + \sigma_b}{d}, \frac{\sigma_b + \rho + \lambda}{d}; \frac{\rho\lambda}{d^2}p(z-1)\right), \quad (19)$$

where ${}_1F_2(\bullet; \bullet, \bullet; \bullet)$ is a generalised hypergeometric function. Note that there exists no renormalization of rates in Eq. (18) that leads to Eq. (19). This is possible only in an approximate sense in the limit of large ρ because as shown in [37] in this case the dynamics of the three-state model (16) converge to those of the telegraph model (10) — this limit physically corresponds to the rapid release of the polymerase from its paused state prior to the start of transcriptional elongation.

Hence, we conclude that generally the solution of a multi-state gene model that accounts for technical noise can be mapped, with an appropriate renormalization of kinetic rates, to the solution of a model with no technical noise, provided there is no change of promoter state upon transcription.

2.2.3 Bursty models of gene product dynamics

An alternative type of commonly used model of gene expression is the bursty model whereby molecules are produced not one at a time but in bursts. Consider the bursty production of molecules (mRNA or proteins) from a promoter in state i and their subsequent degradation



where s is a geometrically distributed random variable with mean $b(t)$, $r(t)$ is the time-dependent burst frequency and $d(t)$ is the time-dependent degradation rate. For mRNAs, this model (with constant kinetic rates) can be

derived from the telegraph model in the limit that the inactivation rate is much larger than the activation rate [47]; this is a common assumption [48]. For proteins, this model (with constant kinetic rates) can be derived from more complex multi-state models of gene expression in the limit that the mRNA lifetime is much less than the protein lifetime [49]. Experimental validation of the geometric or exponential distribution (the continuous analog of the discrete distribution) of the burst size can be found in [50, 51].

The master equation for this model (without technical noise) is given by

$$\frac{d}{dt}Q_i(m, t) = r(t) \sum_{s=0}^{\infty} P_{\text{geo}}(s, t) [Q_i(m-s, t) - Q_i(m, t)] + d(t)((m+1)Q_i(m+1, t) - mQ_i(m, t)), \quad (21)$$

where $P_{\text{geo}}(s, t) = (1 - \alpha(t))^s \alpha(t)$ for $s = 0, 1, 2, \dots$ is the geometric distribution and $\alpha(t) = 1/(1 + b(t))$. The generating function equation in the absence of technical noise is

$$\frac{d}{dt}G_i^*(z, t) = r(t)G_i^*(z, t) \left(\frac{1}{1 + b(t)(1-z)} - 1 \right) - d(t)(z-1) \frac{\partial G_i^*(z, t)}{\partial z}. \quad (22)$$

Upon the change of variable z to $1 - p(1 - z)$ and replacing G_i^* by G_i , we obtain the generating function equation in the presence of technical noise:

$$\frac{d}{dt}G_i(z, t) = r(t)G_i(z, t) \left(\frac{1}{1 + b(t)p(1-z)} - 1 \right) - d(t)(z-1) \frac{\partial G_i(z, t)}{\partial z}. \quad (23)$$

Comparing Eqs. (22) and (23) we see that the addition of technical noise leads to a rescaling of the mean burst size from $b(t)$ to $b(t)p$ but it has no effect on the burst frequency. The special case of time-independent rates leads to a steady-state negative binomial distribution of counts with rescaled burst size [21].

For a more complex system with N promoter states:

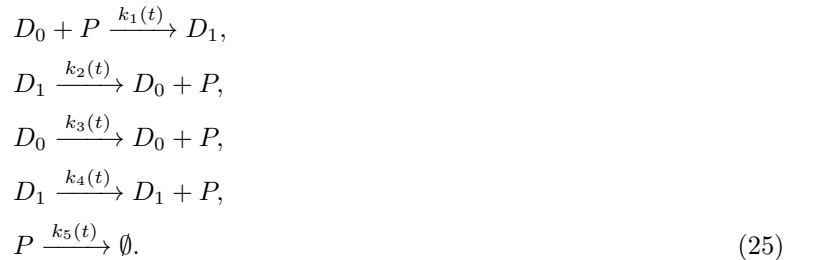


where s_i is a geometrically distributed random number with mean $b_i(t)$, it is straightforward to verify that the effect of technical noise is akin to the renormalization of all burst sizes: $b_i(t) \mapsto b_i(t)p$.

2.3 The influence of technical noise on auto-regulated gene expression

Next, we consider models that explicitly describe transcription factor dynamics. Specifically we consider autoregulation, whereby a gene's protein product serves as its own transcription factor. Examples of such systems abound in nature. For example, it has been estimated that 40% of all transcription factors in *Escherichia coli* self-regulate [52], with the majority of them participating in autorepression [53]. For a review of stochastic models of auto-regulation, the reader is referred to [54].

2.3.1 A simple model of auto-regulation



We consider a simple auto-regulatory genetic feedback loop whereby a promoter can be in two states (D_0 and D_1), protein production is possible from each state (albeit with a different rate), and the promoter state changes

upon protein binding. This models a negative feedback loop if $k_3(t) > k_4(t)$ (since protein binding causes a decrease of the production rate) and a positive feedback loop if $k_3(t) < k_4(t)$ (since protein binding causes an increase of the production rate). We assume that the protein is observed with capture probability p . For simplicity, we have not explicitly modeled the mRNA dynamics.

As before, from the chemical master equation we can write the generating functions for true protein fluctuations conditioned on the state of the promoter [11]:

$$\frac{\partial G_0^*(z, t)}{\partial t} = k_3(t)(z-1)G_0^*(z, t) - k_5(t)(z-1)\frac{\partial G_0^*(z, t)}{\partial z} + k_2(t)zG_1^*(z, t) - k_1(t)z\frac{\partial G_0^*(z, t)}{\partial z}, \quad (26)$$

$$\frac{\partial G_1^*(z, t)}{\partial t} = k_4(t)(z-1)G_1^*(z, t) - k_5(t)(z-1)\frac{\partial G_1^*(z, t)}{\partial z} - k_2(t)G_1^*(z, t) + k_1(t)\frac{\partial G_0^*(z, t)}{\partial z}. \quad (27)$$

Upon the change of variable z to $1 - p(1 - z)$, we find that the generating function equations of the observed protein are given by

$$\begin{aligned} \frac{\partial G_0(z, t)}{\partial t} &= k_3(t)p(z-1)G_0(z, t) - k_5(t)(z-1)\frac{\partial G_0(z, t)}{\partial z} + k_2(t)(1-p(1-z))G_1(z, t) - \frac{k_1(t)}{p}(1-p(1-z))\frac{\partial G_0(z, t)}{\partial z}, \\ \frac{\partial G_1(z, t)}{\partial t} &= k_4(t)p(z-1)G_1(z, t) - k_5(t)(z-1)\frac{\partial G_1(z, t)}{\partial z} - k_2(t)G_1(z, t) + \frac{k_1(t)}{p}\frac{\partial G_0(z, t)}{\partial z}. \end{aligned} \quad (28)$$

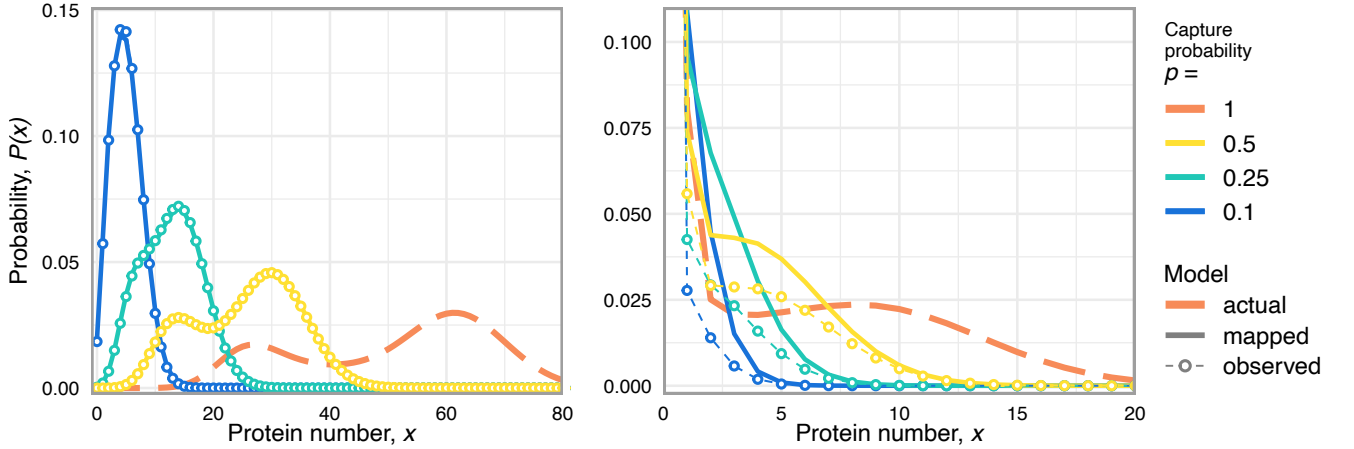


Figure 2: Effect of technical noise on the steady-state marginal distributions of protein numbers in a simple model of an auto-regulatory circuit (25). We consider two sets of time-independent parameters: (a) $k_1 = 0.0025$, $k_2 = 0.3$, $k_3 = 64$, $k_4 = 25$, $k_5 = 1$; (b) $k_1 = 0.5$, $k_2 = 3$, $k_3 = 0.125$, $k_4 = 15$, $k_5 = 1$. The exact steady-state generating function solution $G^*(z) = G_0^*(z) + G_1^*(z)$ for the true protein counts is derived in [11]; for the observed case, it follows by replacing z in these equations by $1 - p(1 - z)$. The exact probability distribution corresponding to the generating function solution, $P(x) = (1/x!)d^x G^*(z)/dz^x|_{z=0}$, are plotted for various capture probabilities $p = 0.1, 0.25, 0.5$ and are shown by open circles; the actual distribution ($p = 1$) is shown by red dashed lines. For comparison, we also show using solid lines, the mapped distributions, i.e., the steady-state distributions obtained for $p = 1$ with renormalized parameters $k_1 \mapsto k_1/p$, $k_3 \mapsto k_3p$ and $k_4 \mapsto k_4p$. Note that the mapped distributions are in excellent agreement with the exact distributions in (a) (solid lines pass through the open circles) but not in (b). This is in agreement with our theory which predicts that the mapping is approximately correct when the protein numbers are sufficiently high — the mean protein abundance is 51.02 in (a) and 2.66 in (b).

Clearly, Eq. (28) does not correspond to Eqs. (26)-(27) with renormalized parameters and hence, generally, the dynamics of the observed system cannot be mapped directly to the dynamics of the true system. However, as we now show this mapping can be done in an approximate sense in the limit of large protein numbers.

Let the n -th derivative of the conditional generating functions be denoted as

$$\mu_n^i(t) = \frac{\partial^n}{\partial z^n} G_i(z, t)|_{z=1} = \sum_x x(x-1)\dots(x-n+1)P_i(x, t), \quad i = 0, 1. \quad (29)$$

These are commonly known as the factorial moments of the system. Using the relation

$$\frac{\partial^n}{\partial z^n} [(z-1)G_i(z, t)] = (z-1)\frac{\partial^n}{\partial z^n} G_i(z, t) + n\frac{\partial^{n-1}}{\partial z^{n-1}} G_i(z, t), \quad (30)$$

it is straightforward to show from Eq. (28) that

$$\begin{aligned}\frac{d\mu_n^0(t)}{dt} &= k_3(t)pn\mu_{n-1}^0(t) - k_5(t)n\mu_n^0(t) + k_2(t)(\mu_n^1(t) + pn\mu_{n-1}^1(t)) - k_1(t)(n\mu_n^0(t) + p^{-1}\mu_{n+1}^0(t)), \\ \frac{d\mu_n^1(t)}{dt} &= k_4(t)pn\mu_{n-1}^1(t) - k_5(t)n\mu_n^1(t) - k_2(t)\mu_n^1(t) + k_1(t)p^{-1}\mu_{n+1}^0(t).\end{aligned}\quad (31)$$

Note that if the condition

$$\mu_n^i(t) \gg pn\mu_{n-1}^i(t), \quad (32)$$

is satisfied then Eq. (31) reduces to

$$\begin{aligned}\frac{d\mu_n^0(t)}{dt} &\approx k_3(t)pn\mu_{n-1}^0(t) - k_5(t)n\mu_n^0(t) + k_2(t)\mu_n^1(t) - k_1(t)p^{-1}\mu_{n+1}^0(t), \\ \frac{d\mu_n^1(t)}{dt} &\approx k_4(t)pn\mu_{n-1}^1(t) - k_5(t)n\mu_n^1(t) - k_2(t)\mu_n^1(t) + k_1(t)p^{-1}\mu_{n+1}^0(t).\end{aligned}\quad (33)$$

These differential equations are a function of $k_1(t)/p$, $k_2(t)$, $k_3(t)p$, $k_4(t)p$ and $k_5(t)$, i.e. the factorial moments of the observed marginal distribution of protein numbers are the same as those of the true system but with renormalized protein production and protein binding rates. In Appendix A we show that, generally, $\mu_n^i(t) \geq \mu_{n-1}^i(t)(\mu_1^i(t) - n + 1)$ from which it follows that a sufficient condition for Eq. (32) to hold is that $\mu_1^i(t) \gg n$. Since the mean protein number conditioned on the DNA state i is $\mu_1^i(t)/\mu_0^i(t)$, it follows that abundance of protein is a sufficient condition for Eq. (32) to approximately hold. These results imply that when regulation is explicitly modeled, not just the production rates are renormalized but the protein binding rate is as well.

These results are confirmed in Fig. 2 using two sets of time-independent parameters. The mapping provides an excellent approximation when the mean protein numbers are high (Fig. 2a) and a poor approximation when it is low (Fig. 2b).

2.3.2 An alternative derivation

An alternative much simpler, though less mathematically rigorous derivation of the same result is possible. We start by making the observation that if proteins are very abundant than the reaction scheme of the auto-regulatory feedback loop (25) can be approximated by the simpler system of reactions



Note that the first reaction has been changed from a bimolecular to a pseudo-first order reaction with a rate equal to a product of $k_1(t)$ and $\langle y|_0(t) \rangle$ the (actual) mean number of proteins conditioned on promoter state D_0 . In the second reaction, we removed production of protein, since an increase of one molecule is negligible when proteins are abundant. The idea is similar in spirit to the Linear-Mapping Approximation of gene regulatory networks [8]. The new effective circuit is a special case of the generalised telegraph model (15) and thus we can immediately deduce that under the influence of technical noise, k_3 changes to k_3p and k_4 changes to k_4p but all other effective rates remain unchanged. Specifically, since the effective rate $k_1(t)\langle y|_0(t) \rangle$ remains unchanged, it follows that $k_1(t)\langle y|_0(t) \rangle = (k_1(t)/p)p\langle y|_0(t) \rangle = (k_1(t)/p)\langle x|_0(t) \rangle$ where in the last step we used the fact that the observed mean number of proteins $\langle x|_i(t) \rangle$ in promoter state D_i is equal to $p\langle y|_i(t) \rangle$ (Eq. (5)). Hence, technical noise leads to a renormalization of the binding rate $k_1(t) \mapsto k_1(t)/p$. Thus the renormalized parameters obtained by this method are in agreement with the results of Section 2.3.1.

The effective circuit describing the observed protein dynamics in the presence of technical noise and assuming

protein abundance is given by

$$\begin{aligned}
D_0 &\xrightarrow{(k_1(t)/p)\langle x|_0(t)\rangle} D_1, \\
D_1 &\xrightarrow{k_2(t)} D_0, \\
D_0 &\xrightarrow{k_3(t)p} D_0 + P, \\
D_1 &\xrightarrow{k_4(t)p} D_1 + P, \\
P &\xrightarrow{k_5(t)} \emptyset.
\end{aligned} \tag{35}$$

2.3.3 The case of fast and slow promoter switching

Fast switching

Let the rates k_i be time-independent constants. The steady-state solution of the model (25) has been previously derived in [11] and the normalisation factor in [55]. Setting k_1 to k_1/δ and k_2 to k_2/δ , and taking the limit $\delta \rightarrow 0$, we obtain the generating function solution of Eqs. (26)-(27) in the limit of fast promoter switching:

$$G^*(z) = \frac{e^{k_4(z-1)} \left(k_3(k_4 + L) {}_1F_1 \left(L - \frac{Lk_3}{k_4}; L + 1; -zk_4 \right) + (k_4 - k_3) L {}_1F_1 \left(-\frac{k_3L}{k_4} + L + 1; L + 1; -zk_4 \right) \right)}{k_3(k_4 + L) {}_1F_1 \left(L - \frac{Lk_3}{k_4}; L + 1; -k_4 \right) + (k_4 - k_3) L {}_1F_1 \left(-\frac{k_3L}{k_4} + L + 1; L + 1; -k_4 \right)}, \tag{36}$$

where $G^*(z) = G_0^*(z) + G_1^*(z)$, $L = k_2/k_1$ and ${}_1F_1(\bullet; \bullet; \bullet)$ is the confluent hypergeometric function.

It is straightforward to see that $G^*(1 - p(1 - z))$ (the exact solution when technical noise is accounted for) is not generally the same as $G^*(z)$ with the renormalized parameters $k_3 \rightarrow k_3p$, $k_4 \rightarrow k_4p$ and $L \rightarrow Lp$. Note that the latter scaling of L comes from the fact that previously our theory suggested $k_1 \mapsto k_1/p$ when technical noise is taken into account. The equivalence between the exact and mapped solutions only occurs when additionally one enforces $L \rightarrow 0$, i.e., when the binding rate is much larger than the unbinding rate. Note that since we are in the fast switching limit this also means that both of these rates are much larger than the production rates.

Note that the constraint of small L does imply that the mean protein number is large (the sufficient condition found in Section 2.3.1). For example, $k_1 = 10^4$, $k_2 = 10^2$, $k_3 = 0.1$, $k_4 = 1$, $k_5 = 1$, $p = 0.3$ leads to an actual steady-state protein mean of 0.29 but the squared relative error between the factorial moments of the actual protein distribution and the mapped protein distribution, summed over the first 5 factorial moments, is merely 6.4×10^{-4} .

Slow switching

In the limit of slow switching rates, i.e., $k_1, k_2 \rightarrow 0$, the generating function solution of Eqs. (26)-(27) reduces to

$$G^*(z) = \frac{Le^{k_3(z-1)} + k_3e^{k_4(z-1)}}{k_3 + L}. \tag{37}$$

This corresponds to a mixture of two Poisson distributions, one corresponding to each promoter state [56, 57]. It is straightforward to see that $G^*(1 - p(1 - z))$ (the exact solution when we account for technical noise) is generally the same as $G^*(z)$ with the renormalized parameters $k_3 \rightarrow k_3p$, $k_4 \rightarrow k_4p$ and $L \rightarrow Lp$. Note that slow switching also does not place a constraint on the mean protein number and hence in this case the mapping is valid even if protein is not abundant. For example, $k_1 = 10^{-3}$, $k_2 = 10^{-3}$, $k_3 = 5$, $k_4 = 1$, $p = 0.3$ leads to a steady-state protein mean of 0.50 but the squared relative error between the factorial moments of the actual protein distribution and the mapped protein distribution, summed over the first 5 factorial moments, is merely 2.7×10^{-5} .

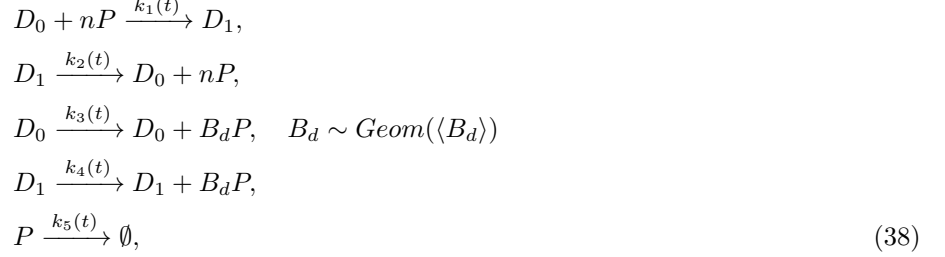
2.3.4 Summary

Hence, we conclude that under the influence of technical noise and for sufficiently high protein abundance, the stochastic protein dynamics of the auto-regulatory circuit (25) is well approximated by the the dynamics of the same circuit without technical noise but with the parameter rescalings $k_1 \mapsto k_1/p$, $k_3 \mapsto k_3p$ and $k_4 \mapsto k_4p$. This results holds for the general case of time-dependent kinetic rates. For the special case where these rates are time-independent constants, we have further shown that the rescaling above holds without necessarily invoking high protein abundance provided timescale separation is enforced. Specifically, this occurs when either the binding and unbinding rates of the protein to the promoter are very small compared to the rest of the rates (slow switching) or

else when binding is much faster than unbinding and both processes are much faster than the remaining reactions (a special case of fast-switching). An extension of these calculations to the case of cell-specific capture probabilities is discussed in Appendix B.

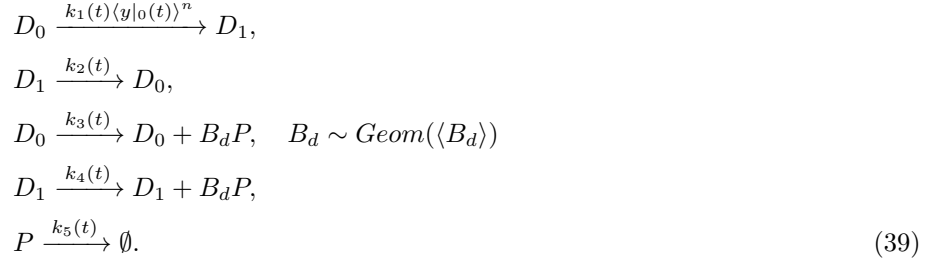
2.4 The influence of technical noise on a more complex model of auto-regulation

Next, we consider a more biologically realistic model of auto-regulation, whereby n proteins are needed to bind to a promoter to cause a change of promoter state and protein is produced not one at a time but in bursts. The reaction scheme is given by



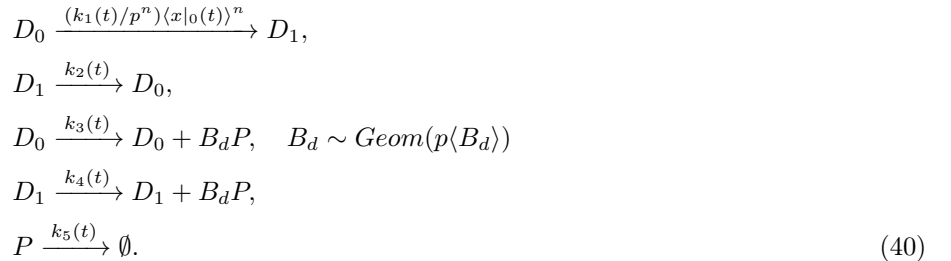
where the burst size B_d is drawn from the geometric distribution with a mean $\langle B_d \rangle$.

Using the logic of Section 2.3.2, we make the observation that if proteins are very abundant than the reaction scheme effectively simplifies to



The new effective circuit is a special case of the generalised bursty model (24) and thus we can immediately deduce that under the influence of technical noise, the mean burst size $\langle B_d \rangle$ changes to $p\langle B_d \rangle$ but all other effective rates remain unchanged. In particular, since the effective rate $k_1(t)\langle y|_0(t) \rangle^n$ is unchanged, it follows that $k_1(t)\langle y|_0(t) \rangle^n = (k_1(t)/p^n)p^n\langle y|_0(t) \rangle^n = (k_1(t)/p^n)\langle x|_0(t) \rangle^n$ where in the last step we used the fact that the observed mean number of proteins $\langle x|_i(t) \rangle$ in promoter state D_i is equal to $p\langle y|_i(t) \rangle$ (Eq. (5)). This implies that technical noise leads to renormalization of the binding rate: $k_1(t) \mapsto k_1(t)/p^n$.

Hence, the effective circuit describing the observed protein dynamics in the presence of technical noise and assuming protein abundance is given by



In principle, more complex gene regulatory circuits can be analyzed in a similar way but we shall not follow this approach further in this paper.

3 Protein distribution prediction under technical noise using a piecewise deterministic approach

In this section we describe an alternative approach to understanding the influence of technical noise on the dynamics of gene regulatory networks. This approach is based on the piecewise deterministic framework of Friedmann et al. [58] which is an approximation of the discrete approach when molecule numbers are sufficiently large.

3.1 General framework

We start by considering the case of no technical noise. We define the protein concentration $y(t)$ by setting $y(t) = P(t)/V$, where $P(t)$ is the protein count and V is the average cell volume. We assume that the concentration of each protein is a continuous random variable that changes discontinuously in time when a production burst occurs. In between consecutive bursts, the protein concentration decays deterministically. Note that we will not explicitly model the mRNA dynamics; rather we assume that since mRNA typically degrades much faster than proteins, the mRNA fluctuations implicitly manifest in the protein burst size distribution [49]. Thus, we obtain a piecewise-deterministic Markov process (PDMP) [59, 60], where synthesis events become instantaneous random jumps (which we call concentration bursts) and protein decay is deterministic. The process is Markov because the time and size of the next jump depend only on the current state of the system.

The probability density function of the random vector $\vec{y} \in \mathbb{R}^N$ is then governed by the Chapman–Kolmogorov equation:

$$\frac{\partial}{\partial t} Q(\vec{y}, t) = - \sum_{i=1}^N \frac{\partial}{\partial y_i} (A_i(\vec{y}, t) Q(\vec{y}, t)) + \int_{[\vec{0}, \vec{y}]} W(\vec{y} | \vec{y}', t) Q(\vec{y}', t) d\vec{y}' - \int_{[\vec{y}, \infty)} W(\vec{y}' | \vec{y}, t) Q(\vec{y}, t) d\vec{y}', \quad (41)$$

where the jump kernel $W(\vec{y} | \vec{y}', t)$ describes the jump-rate density from state \vec{y}' to \vec{y} at time t and the initial distribution is given by $Q(\vec{y}, 0) = Q_0(\vec{y})$. Here, the first term involving $A(\vec{y}, t)$ describes the deterministic dynamics (due to protein degradation) while the integral terms describe the random discontinuous jumps due to bursty protein synthesis (first integral is a gain term and the second integral is a loss term). Note that the corresponding deterministic dynamics between jumps are effectively governed by the differential equation $\partial \langle y_i \rangle / \partial t = A_i(\langle \vec{y} \rangle)$, where $\langle y_i \rangle$ is the mean of the random variable y_i .

3.2 Extending the framework to include technical noise

Next, we extend our piecewise deterministic approach to include a continuous analogue to the discrete binomial capture model described in Section 2.1. For clarity, we first describe it for the case of a single species.

The binomial distribution of observing a protein number z given that the actual number is w is

$$P_{\text{bin}}^p(z|w) = \binom{w}{z} p^z (1-p)^{w-z}. \quad (42)$$

The mean and variance of this distribution are pw and $p(1-p)w$, respectively. Assuming abundant molecule numbers, this is well approximated by a Gaussian:

$$\phi(z|w, p) = \frac{1}{\sqrt{2\pi p(1-p)w}} \exp \left\{ -\frac{(z - pw)^2}{2p(1-p)w} \right\}. \quad (43)$$

Switching to the (continuous) concentrations, $x \rightarrow z/V$ and $y \rightarrow w/V$, the distribution becomes

$$\phi(x|y, p) = \sqrt{\frac{V}{2\pi p(1-p)y}} \exp \left[-V \frac{(x - py)^2}{2p(1-p)y} \right]. \quad (44)$$

Following Eq. (1), the distribution of the observed protein concentration is given by:

$$P(x, t) = \int_{\mathbb{R}} \phi(x|y, p) Q(y, t) dy. \quad (45)$$

Next, we approximate this integral using Laplace's method [61]. Consider an integral of the form

$$I(V) = \int_a^b f(y) e^{-Vg(y)} dy, \quad a < b, \quad a, b \in \mathbb{R}, \quad (46)$$

and assume that g has a unique nondegenerate minimum at an interior point y_0 with $g'(y_0) = 0$ and $g''(y_0) > 0$. According to Laplace's method as $V \rightarrow \infty$, the integral is well approximated by

$$I(V) \sim f(y_0) e^{-Vg(y_0)} \sqrt{\frac{2\pi}{Vg''(y_0)}}. \quad (47)$$

Comparing Eqs. (44)-(45) with Eq. (46), we see that in our case,

$$g(y) = \frac{(x - py)^2}{2p(1-p)y}, \quad f(y) := \sqrt{\frac{V}{2\pi p(1-p)y}} Q(y, t). \quad (48)$$

The stationary point satisfies $g'(y) = 0$, giving

$$y_0 = \frac{x}{p} > 0, \quad g(y_0) = 0, \quad g''(y_0) = \frac{p}{(1-p)y_0}.$$

Applying Laplace's approximation, Eq. (47), we obtain

$$P(x, t) \sim \frac{1}{p} Q\left(\frac{x}{p}, t\right), \quad V \rightarrow \infty. \quad (49)$$

Note that the assumption of large V is akin to taking the macroscopic limit of the system. Note also that this implies that the mean and variance of the observed and actual distributions are related by

$$\begin{aligned} \mu_x &= p\mu_y, \\ \sigma_x^2 &= p^2\sigma_y^2. \end{aligned}$$

Comparing with the relationships derived from the discrete model (Eq. (5)-(6)), we see that the Laplace approximation gives the correct mean but the variance is only approximately correct provided the Fano factor of the actual distribution satisfies the inequality $FF_y = \sigma_y^2/\mu_y \gg (1-p)/p$. Fano factors of actual distributions are typically in the range 1 – 10 [62] and hence Eq. (49) is only a useful approximation provided p is not too small.

The framework above for a single protein species can be straightforwardly generalized to the case of N proteins. The observation kernel (Eq. (44)) becomes a multivariate normal distribution with the mean $\vec{\mu} = (p_1 y_1, \dots, p_N y_N)$ and the covariance matrix Σ . Since we assume that observations of protein i and j are independent, Σ becomes diagonal with $\Sigma_{ii} = p(1-p)y_i$; then $\phi(\vec{x}|\vec{y}, \vec{p}) = \prod_{i=1}^N \phi(x_i|y_i, p_i)$. This allows us to repeat the calculations above and obtain the approximation for the joint pdf of observed protein concentrations $P(\vec{x}, t)$:

$$P(x_1, \dots, x_N) \approx \frac{1}{p_1 \dots p_N} Q\left(\frac{x_1}{p_1}, \dots, \frac{x_N}{p_N}, t\right), \quad (50)$$

where x_i and p_i are the observed concentration and the capture probability for the i -th protein species, respectively. Hence, it follows that the derivatives of $Q(\vec{y}, t)$ and $P(\vec{x}, t)$ are related as follows: $\partial Q/\partial t = (\Pi_i p_i) \partial P/\partial t$, $\partial/\partial y_i = p_i \partial/\partial x_i$. Using these relationships and Eq. (41), we can write the Chapman-Kolmogorov equation for the distribution of the observed protein concentration $P(\vec{x}, t)$:

$$\begin{aligned} \frac{\partial P(\vec{x}, t)}{\partial t} &= - \sum_{i=1}^N \frac{\partial}{\partial x_i} \left(p_i A_i(\vec{x}_p, t) P(\vec{x}, t) \right) \\ &\quad + \int_{[0, \vec{x}]} \frac{1}{\prod_{k=1}^N p_k} W(\vec{x}_p | \vec{x}'_p, t) P(\vec{x}', t) d\vec{x}' - \int_{[\vec{x}, \infty)} \frac{1}{\prod_{k=1}^N p_k} W(\vec{x}'_p | \vec{x}_p, t) P(\vec{x}, t) d\vec{x}' \end{aligned} \quad (51)$$

where \vec{x}_p is a short notation for component-wise divided vector \vec{x} by \vec{p} , i.e., $\vec{x}_p = \left(\frac{x_1}{p_1}, \dots, \frac{x_N}{p_N}\right)$.

3.3 Application I: Bursty Protein expression — no explicit regulatory dynamics

$$\begin{aligned} \emptyset &\xrightarrow{\alpha(t)} Y \cdot B, \quad B \sim \text{Exp}(1/\beta), \\ Y &\xrightarrow{\gamma(t)} \emptyset \end{aligned} \quad (52)$$

Consider a simple model of gene expression where the protein concentration changes due to production and decay. Protein production occurs randomly at a rate $\alpha(t)$ and causes instantaneous jumps (bursts) in the protein concentration. In agreement with experiments [51], previous theoretical work [58], and the discrete bursty model approach

of Section 2.2.3, it is assumed that each concentration burst is drawn from an exponential distribution with a mean β . The corresponding jump kernel is:

$$W(y | y', t) = \frac{1}{\beta} e^{-\frac{y-y'}{\beta}} \alpha(t), \quad y' < y, \quad (53)$$

From Eq. (41) it follows that the Chapman-Kolmogorov equation describing the time-evolution of the distribution of the actual protein concentration is

$$\frac{\partial Q(y, t)}{\partial t} = \frac{\partial}{\partial y} (\gamma(t) y Q(y, t)) + \frac{\alpha(t)}{\beta} \int_0^y e^{-\frac{y-y'}{\beta}} Q(y', t) dy' - \alpha(t) Q(y, t). \quad (54)$$

Note that $A(y)$ in Eq. (41) equals $-\gamma(t)y(t)$ since the protein concentration y decays according to first-order kinetics with a rate $\gamma(t)$ in between concentration jumps due to protein synthesis.

Similarly, from Eq. (51) it follows that the corresponding Chapman-Kolmogorov equation for the distribution of the observed protein concentration $P(x, t)$ is

$$\frac{\partial P(x, t)}{\partial t} = \frac{\partial}{\partial x} (\gamma(t) x P(x, t)) + \frac{\alpha(t)}{p\beta} \int_0^x e^{-\frac{x-x'}{p\beta}} P(x', t) dx' - \alpha(t) P(x, t). \quad (55)$$

Comparing Eqs. (54) and (55), we see that the two equations have the same structure, except that the jump size is effectively renormalized by p : $\beta \mapsto p\beta$. This result parallels that proved using the discrete approach based on the chemical master equation in Section 2.2.3.

3.4 Application II: Protein dynamics of an auto-regulated gene

In this section, we consider again the autoregulatory model studied earlier (scheme (38)). The reaction scheme for a discrete model of this type is



where P is the protein, and D_0 and D_1 denote a promoter in unbound and bounded states, respectively. As before, we will assume one gene copy. The burst size B_d is drawn from the geometric distribution; the subscript d stands for discrete.

In what follows, we first simplify the model under the assumption of fast switching promoter state dynamics. We start by deducing the effective protein production and degradation rates. Writing the deterministic rate equations for the (approximate) means of the unbound promoter and protein numbers, $\langle D_0(t) \rangle$ and $\langle P(t) \rangle$, respectively, and applying the fast-equilibrium approximation (i.e. $d\langle D_0 \rangle/dt \approx 0$), we obtain:

$$\langle D_0(t) \rangle \approx \frac{K_d^n(t)}{K_d^n(t) + \langle P(t) \rangle^n}, \quad K_d^n(t) = \frac{\sigma_u(t)}{\sigma_b(t)}.$$

Note that $\sigma_u(t)/\sigma_b(t)$ is the dissociation constant of the protein-promoter reaction. Note that here we assumed that the time dependence of the binding and unbinding rates is weak such that a quasi-equilibrium between promoter and protein can be reached. Hence, it follows that the (approximate) deterministic time evolution of the mean protein number $\langle P(t) \rangle$ is given by

$$\frac{d\langle P(t) \rangle}{dt} \approx \langle B_d \rangle \alpha(\langle P(t) \rangle, t) - d(t) \langle P(t) \rangle, \quad \alpha(\langle P(t) \rangle, t) = \frac{\rho_u(t) K_d^n(t) + \rho_b(t) \langle P(t) \rangle^n}{K_d^n(t) + \langle P(t) \rangle^n}.$$

Similar equations can be written for the protein concentration $y(t) = P(t)/V$. This rate equation suggests an effective PDMP with reaction scheme



where

$$\alpha(y, t) = \frac{\rho_u(t)K^n(t) + \rho_b(t)y^n(t)}{K^n(t) + y^n(t)}, \quad \gamma(t) = d(t), \quad (58)$$

and $K(t) = K_d(t)/V$. Note that the concentration burst size B is drawn from the exponential distribution with mean $\beta = \langle B_d \rangle / V$ (the exponential distribution is the continuous analog of the geometric distribution used in the discrete model with scheme (56)).

The jump kernel is $W(y | y', t) = \frac{1}{\beta} e^{-\frac{y-y'}{\beta}} \alpha(y', t)$ for $y' < y$. Hence, the Chapman-Kolmogorov equation (Eq. (41)) for the dynamics of the distribution of the actual protein concentration is given by

$$\frac{\partial Q(y, t)}{\partial t} = \frac{\partial}{\partial y} (\gamma(t)yQ(y, t)) + \frac{1}{\beta} \int_0^y \alpha(y, t) e^{-\frac{y-y'}{\beta}} Q(y', t) dy' - \alpha(y, t)Q(y, t). \quad (59)$$

Using Eq. (51) it follows that the corresponding Chapman-Kolmogorov equation for the dynamics of the distribution of the observed protein concentration $P(x, t)$ is

$$\frac{\partial P(x, t)}{\partial t} = \frac{\partial}{\partial x} (\gamma(t)xP(x, t)) + \frac{1}{p\beta} \int_0^x \alpha(x/p, t) e^{-\frac{x-x'}{p\beta}} P(x', t) dx' - \alpha(x/p, t)P(x, t). \quad (60)$$

A comparison of the two equations above implies that technical noise causes a renormalization of the mean burst size ($\beta \mapsto p\beta$); evaluation of the feedback rate $\alpha(y, t)$ (Eq. (58)) at $y = x/p$ yields a renormalization of the constant K ($K \mapsto pK$). Hence, the effective PDMP model corresponding to the new Chapman-Kolmogorov equation (60) is given by

$$\begin{aligned} \emptyset &\xrightarrow{\tilde{\alpha}(x, t)} X \cdot B, \quad B \sim \text{Exp}(1/p\beta), \\ X &\xrightarrow{\gamma(t)} \emptyset, \end{aligned} \quad (61)$$

where

$$\tilde{\alpha}(x, t) = \frac{\rho_u(t)p^n K^n(t) + \rho_b(t)x^n(t)}{p^n K^n(t) + x^n(t)}, \quad \gamma(t) = d(t). \quad (62)$$

Note that these results are compatible with those obtained earlier using the discrete approach of Section 2.4 since $K \mapsto pK$ is the same as $K^n \mapsto p^n K^n$ which is compatible with a rescaling of the binding rate: $\sigma_b \mapsto \sigma_b/p^n$.

In Fig. 3 we test the accuracy of our theory by means of stochastic simulations. For a parameter set, we use hybrid Gillespie simulations to simulate the “true” observed process — the PDMP corresponding to the reaction scheme (57) with its output passed through a probabilistic observation model defined by the measurement kernel Eq. (44). For the same parameter set, we use hybrid Gillespie simulations to simulate the predicted observed process — the PDMP corresponding to the reaction scheme (61). We find that the time-dependent distributions from these two simulations are in excellent agreement over a wide range of capture probabilities p and for all times. The algorithm and details of the hybrid Gillespie method are provided in Appendix C.

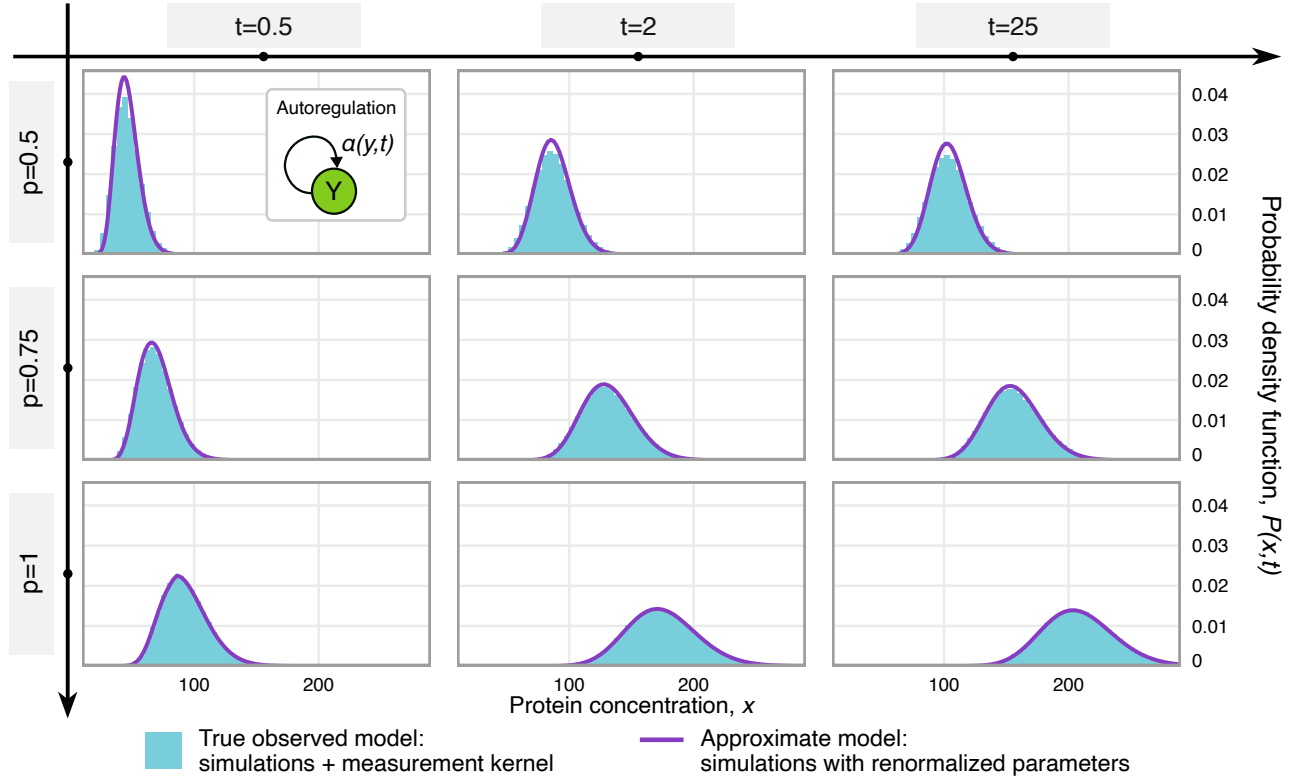


Figure 3: Testing the validity of an approximate model for protein distribution dynamics in an autoregulatory loop (56) with technical noise. The parameters are chosen so that the circuit displays positive feedback — the circuit is illustrated by a cartoon in the top left corner. The probability of observing a protein is denoted by p . The light blue histograms show the “true” observed distributions — these are generated by hybrid-Gillespie algorithm simulations corresponding to the reaction scheme (57) and whose output is passed through a probabilistic observation model defined by the measurement kernel Eq. (44) to simulate technical noise. The solid purple lines show the predictions of the hybrid Gillespie algorithm simulations corresponding to the effective reaction scheme (61) which accounts implicitly for technical noise through a renormalization of parameters derived using our theory. The coincidence of the solid lines and histograms verifies the accuracy of the theory for wide range of values of p and in time. Specifically, this shows that the protein dynamics in the presence of technical noise are equivalent to the dynamics in the absence of technical noise but with renormalized parameters. The parameter values used in the simulations are: $\beta = 4$, $K = 10^3$, $\rho_u = 12$, $\rho_b = 52$, $n = 3$, $\gamma = 1$. Initial conditions: (i) for the true model, $N(\mu, \sigma^2)$ with $\mu = 60$, $\sigma = 25$; (ii) for the approximate model, $N(p\mu, p^2\sigma^2)$ as follows from Eq. (50). In all cases, distributions were estimated from 10^5 simulation runs.

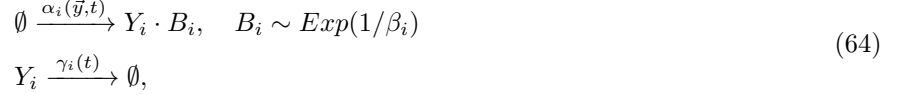
3.5 Application III: Protein dynamics of a general gene regulatory network

Finally, we consider a model of a general gene regulatory network consisting of N interacting genes. For flexibility, we allow the protein from each gene to bind with some probability all genes. The set of reactions that the i -th promoter and protein is involved in is given by

$$\begin{aligned}
 D_{0,i} + \sum_{j=1}^N n_{ij} P_j &\xrightarrow{\sigma_{b,i}(t)} D_{1,i}, \\
 D_{1,i} &\xrightarrow{\sigma_{u,i}(t)} D_{0,i} + \sum_{j=1}^N n_{ij} P_j, \\
 D_{0,i} &\xrightarrow{\rho_{u,i}(t)} D_{0,i} + B_{d,i} \cdot P_i, \\
 D_{1,i} &\xrightarrow{\rho_{b,i}(t)} D_{1,i} + B_{d,i} \cdot P_i, \\
 P_i &\xrightarrow{d_i(t)} \emptyset.
 \end{aligned} \tag{63}$$

Here $D_{0,i}$ and $D_{1,i}$ denote the unbound and bound states of the i -th promoter, respectively; n_{ij} is the number of molecules of protein j required to bind the unbound promoter of protein i to cause a state change; $B_{d,i}$ is the random burst size for protein i ; $d_i(t)$ is the degradation rate. We assume a single gene copy of each protein so that $D_{0,i}(t) + D_{1,i}(t) = 1$.

Following the model reduction approach of Section 3.4, we find that the effective reaction scheme for the dynamics of the i -th protein is given by



with the effective burst frequency α_i and the degradation rate γ_i given by

$$\alpha_i(\vec{y}, t) = \frac{\rho_{u,i}(t)K_i(t) + \rho_{b,i}(t)\prod_{j=1}^N y_j^{n_{ij}}(t)}{K_i(t) + \prod_{j=1}^N y_j^{n_{ij}}(t)}, \quad \gamma_i(t) = d_i(t). \quad (65)$$

where $K_i = \sigma_{u,i}/\sigma_{b,i}$. Note that the concentration burst size B_i is drawn from the exponential distribution with mean $\beta_i = \langle B_{d,i} \rangle / V$.

To obtain the jump kernel $W(\vec{y} | \vec{y}')$, we first note that the jump kernel for a single species i is given by

$$W_i(\vec{y} | \vec{y}') = \frac{1}{\beta_i} e^{-\frac{y_i - y'_i}{\beta_i}} \alpha_i(\vec{y}', t) \prod_{j \neq i} \delta(y_j - y'_j), \quad y' < y,$$

which shows that during the synthesis reaction only molecules of the i -th protein species are produced and other species are not affected. Since bursts occur independently, the jump kernel $W(\vec{y} | \vec{y}')$ is given by

$$W(\vec{y} | \vec{y}') = \sum_{i=1}^N W_i(\vec{y} | \vec{y}'). \quad (66)$$

Hence, the Chapman-Kolmogorov equation describing the dynamics of the distribution of the actual concentration vector, $Q(\vec{y}, t)$, is given by

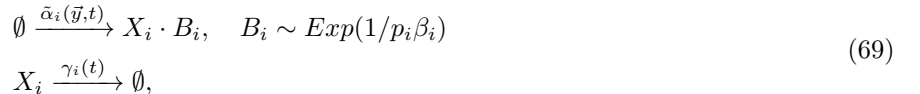
$$\frac{\partial Q(\vec{y}, t)}{\partial t} = \sum_{i=1}^N \frac{\partial}{\partial y_i} (\gamma_i(t) y_i Q(\vec{y}, t)) + \sum_{i=1}^N \int_0^{y_i} \frac{e^{-(y_i - y'_i)/\beta_i}}{\beta_i} \alpha_i(\vec{y}^{(i)}, t) Q(\vec{y}^{(i)}, t) dy'_i - Q(\vec{y}, t) \sum_{i=1}^N \alpha_i(\vec{y}, t), \quad (67)$$

where $\vec{y}^{(i)} = (y_1, \dots, y_{i-1}, y'_i, y_{i+1}, \dots, y_N)$ denotes the state of the system before the concentration burst of protein i — thus the i -th integral accounts for the probability influx due to bursts of protein i .

Finally, using Eq. (51), we obtain the corresponding Chapman-Kolmogorov equation for the distribution of the observed concentration vector, $P(\vec{x}, t)$:

$$\frac{\partial P(\vec{x}, t)}{\partial t} = \sum_{i=1}^N \frac{\partial}{\partial x_i} (\gamma_i(t) x_i P(\vec{x}, t)) + \sum_{i=1}^N \int_0^{x_i} \frac{e^{-(x_i - x'_i)/(p_i \beta_i)}}{p_i \beta_i} \alpha_i(\vec{x}_p^{(i)}, t) P(\vec{x}^{(i)}, t) dx'_i - P(\vec{x}, t) \sum_{i=1}^N \alpha_i(\vec{x}_p, t), \quad (68)$$

where $\vec{x}^{(i)} = (x_1, \dots, x_{i-1}, x'_i, x_{i+1}, \dots, x_N)$ and $\vec{x}_p^{(i)} = (\frac{x_1}{p_1}, \dots, \frac{x_{i-1}}{p_{i-1}}, \frac{x'_i}{p_i}, \frac{x_{i+1}}{p_{i+1}}, \dots, \frac{x_N}{p_N})$. Hence, it follows that the parameter mapping follows $\beta_i \mapsto p_i \beta_i$ and $K_i \mapsto K_i \prod_{j=1}^N p_j^{n_{ij}}$, which is consistent with the single species result in Eq. (60). The effective PDMP model corresponding to the new Chapman-Kolmogorov equation is given by



with the effective burst frequency $\tilde{\alpha}_i$ and the degradation rate γ_i given by

$$\tilde{\alpha}_i(\vec{y}, t) = \frac{\rho_{u,i}(t)K_i(t)\prod_{j=1}^N p_j^{n_{ij}} + \rho_{b,i}(t)\prod_{j=1}^N x_j^{n_{ij}}(t)}{K_i(t)\prod_{j=1}^N p_j^{n_{ij}} + \prod_{j=1}^N x_j^{n_{ij}}(t)}, \quad \gamma_i(t) = d_i(t). \quad (70)$$

In Fig. 4 and Fig. 5 we test the accuracy of our theory by means of stochastic simulations of the two gene toggle switch [63] and the three gene repressilator, respectively [64] — these are special cases of the general gene regulatory network (63). We use hybrid Gillespie simulations to simulate the “true” observed process — the PDMP corresponding to the reaction scheme (64) with its output passed through a probabilistic observation model defined by the measurement kernel Eq. (44). We also use the hybrid Gillespie simulations to simulate the predicted observed process — the PDMP corresponding to the reaction scheme 69. We find that for both gene regulatory networks, the time-dependent distributions from these two simulations are in excellent agreement over a wide range of capture probabilities p and for all times. Breakdown becomes apparent for small enough p as shown in Fig. 5C. For the repressilator, since this circuit can produce sustained oscillations in the protein concentrations, we also investigate the normalised power spectra and find that simulations of the true and predicted observed processes lead to similar predictions except when p is very small (Fig. 5D-F).

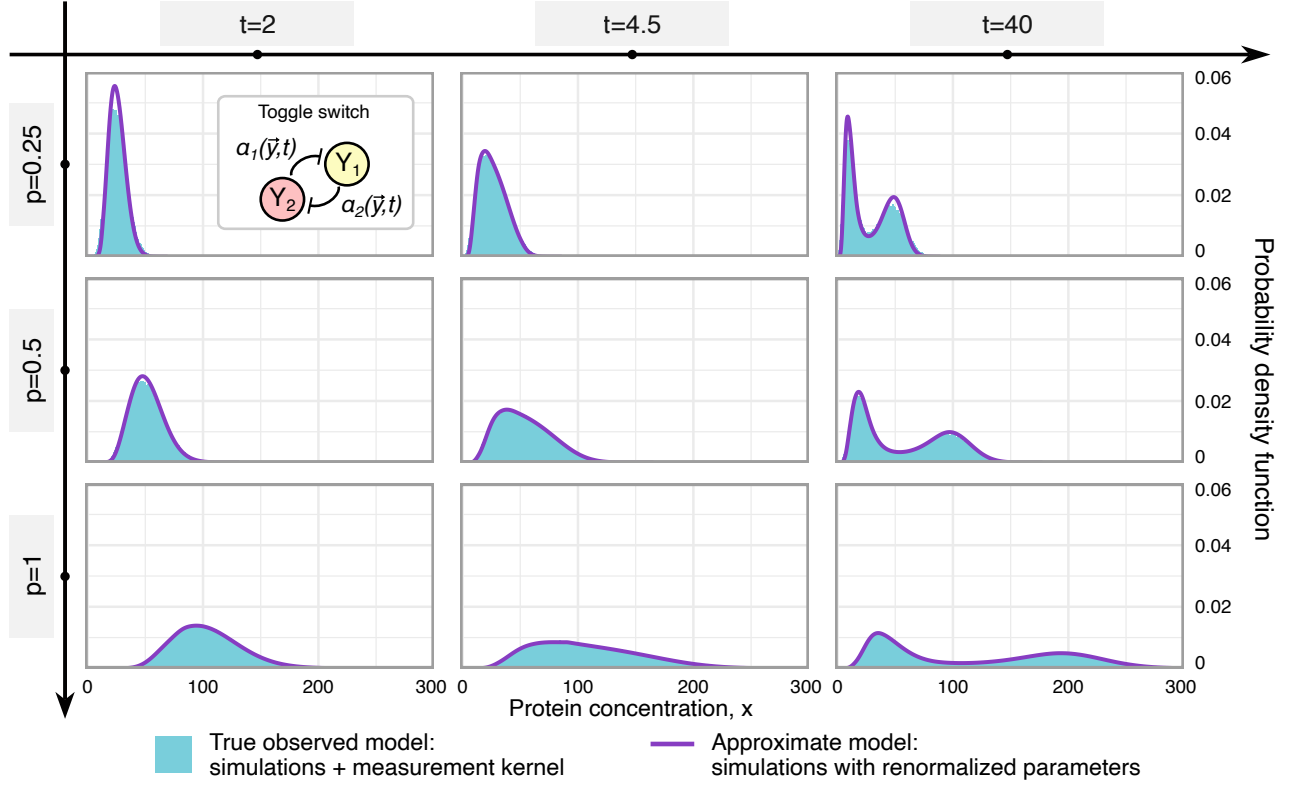


Figure 4: Testing the validity of an approximate model for protein distribution dynamics in a two gene toggle switch with technical noise. The circuit is illustrated by a cartoon in the top left corner. This is a symmetric toggle switch in the sense that species y_1 and y_2 mutually repress each other with rates α_1 and α_2 that have identical parameter values; the capture probabilities are also assumed to be equal $p_1 = p_2 = p$. By symmetry, the protein distributions are equal and hence, we show only the distribution of one of the species. The light blue histograms show the “true” observed distributions — these are generated by hybrid-Gillespie algorithm simulations corresponding to the reaction scheme (64) and whose output is passed through a probabilistic observation model defined by the measurement kernel Eq. (44)) to simulate technical noise. The solid purple lines show the predictions of the hybrid Gillespie algorithm simulations corresponding to the effective reaction scheme (69) which accounts implicitly for technical noise through a renormalization of parameters derived using our theory. The coincidence of the solid lines and histograms verifies the accuracy of the theory for wide range of values of p and in time. Specifically, this shows that the protein dynamics in the presence of technical noise are equivalent to the dynamics in the absence of technical noise but with renormalized parameters. The parameter values used in the simulations are: $\beta_1 = \beta_2 = 3$, $K_1 = K_2 = 7200$, $\rho_{u,1} = \rho_{u,2} = 81.235$, $\rho_{b,1} = \rho_{b,2} = 1.11$, $n_{11} = n_{22} = 0$, $n_{12} = n_{21} = 2$, $\gamma_1 = \gamma_2 = 1$. Initial conditions: (i) for the true model, a bivariate normal distribution with $\bar{\mu} = (120, 120)$ and $\Sigma = \text{diag}(10^2, 10^2)$; (ii) for the approximate model, the distribution follows from Eq. (50). In all cases, distributions were estimated from 10^5 simulation runs.

4 Conclusion

In this paper, we have modeled the impact of technical noise due to imperfect molecular capture on the stochastic dynamics of GRNs. This was achieved using two complementary frameworks: (i) the chemical master equation, which fully captures the discrete nature of molecular events; (ii) a PDMP approach, which retains only a partial description of molecular discreteness and which assumes fast promoter switching.

For systems with non-explicit regulatory interactions, i.e., those which do not explicitly model transcription factor binding interactions, and which additionally do not effectively model promoter-proximal pausing, both methods give the same results. If synthesis occurs a molecule at a time then the synthesis rate ρ is renormalized to ρp where p is the capture probability. If synthesis occurs in bursts whose size is geometrically or exponentially distributed then the mean burst size b is renormalized to $b p$. These results imply that technical noise leads to an *apparent reduction* in either the synthesis rate or the mean burst size. These hold regardless of the number of promoter states or the structure of the promoter-state graph, and remain valid even when the kinetic rates are time-dependent. In models with no explicit modeling of regulatory interactions but where proximal-promoter pausing is effectively modeled, technical noise does not generally correspond to a renormalization of rates, except in the special limit where the pause is short-lived.

For systems with explicit regulatory interactions, i.e., those which explicitly model transcription factor binding interactions leading to auto-regulation or cross-regulation, analytical progress is possible for general GRNs using

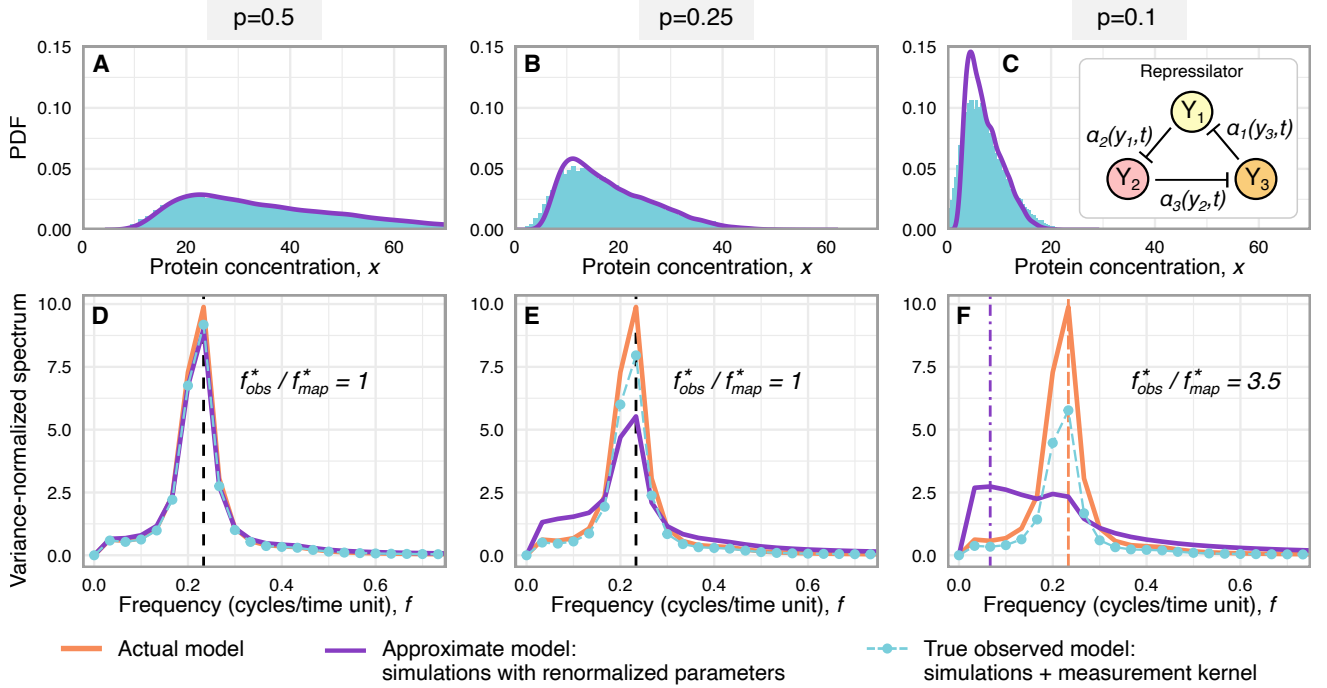


Figure 5: Testing the validity of an approximate model for protein statistics in a three-gene repressilator with technical noise. The circuit is shown in the top-right cartoon. All three genes share identical reaction rates $\alpha_i(\vec{y}, t)$ and capture probabilities p_i , so their protein statistics are identical; only the statistics for one species is shown. (A–C) Light-blue histograms show the “true” observed distributions obtained by hybrid-Gillespie simulations of reaction scheme (64), with technical noise added via the measurement kernel in Eq. (44). Solid purple curves show predictions from hybrid-Gillespie simulations of the effective reaction scheme (69), which incorporates technical noise through theoretically derived renormalized parameters. The agreement between curves and histograms confirms the validity of the approximation for moderate p , with a clear breakdown at $p = 0.1$. (D–F) Average one-sided periodograms of protein time series, normalized by the sample variance; orange, violet, and blue correspond to actual, predicted-observed, and true-observed trajectories, respectively. For $p \geq 0.5$, the normalized spectra are approximately invariant to technical noise. The dominant frequency f^* is accurately predicted for $p \geq 0.25$ but underestimated for small p , where the predicted spectrum becomes broad and loses apparent oscillations, unlike the true observed spectrum which remains sharply peaked. Parameters: $\beta_i = 2$, $K_i = 7 \times 10^4$, $\rho_{u,i} = 130$, $\rho_{b,i} = 2.9$, $\gamma_i = 1$, $n_{13} = n_{21} = n_{32} = 3$. Distributions estimated from 5×10^4 simulations. Periodogram settings: $T = 30$, $\Delta t = 0.01$, $\Delta f = 1/30$, $f_{\text{Nyquist}} = 50$.

the PDMP approach; the special case of auto-regulation is also analytically tractable using the chemical master equation approach. All approaches show that in the limit of protein abundance, besides the scaling of the synthesis or burst sizes as discussed above, there is an additional scaling of the transcription factor binding rates. Specifically, for a protein-promoter binding reaction of the type



where N different proteins can bind to a free promoter causing a change of its state from D_0 to D_1 , the rate constant $k(t)$ is renormalized to $k(t)/\prod_{j=1}^N p_j^{n_j}$, where p_j is the capture probability of the j -th protein and n_j is a non-negative integer equal to the number of proteins of P_j that bind to the promoter. These results imply that technical noise leads to an *apparent amplification* of the rate at which protein binding reactions occur. Discrete modeling of auto-regulation using the chemical master equation also suggests that the rescaling still holds without assuming high protein abundance, when protein–promoter binding and unbinding are much slower than all other reactions (slow switching), or when binding is much faster than unbinding and both processes are much faster than the remaining reactions (a special case of fast-switching).

We note that while our calculations assumed that each cell has the same capture probability p for a specific molecular species, as shown in Appendix B, all our rate renormalization results still hold for the general case of non-identical cells with an associated distribution of capture probabilities. The difference is simply that the renormalization is now cell-specific, i.e., using the capture probabilities specific to a particular cell.

Concluding, our kinetic parameter renormalization results offer a principled foundation for interpreting noisy single-cell data. We anticipate that this framework will open the door to new inference strategies for GRN param-

eters that explicitly and accurately correct for technical noise, thereby enabling more reliable quantitative insight into gene regulatory dynamics.

Acknowledgments

R. G. acknowledges support from the Leverhulme Trust (RPG-2024-082). I. Z. is funded by the EU NextGenerationEU through the Recovery and Resilience Plan for Slovakia under the project No. 09I03-03-V05-00012.

Appendix A Proof of an important inequality

Here we prove that

$$\langle x^{(n)} \rangle \geq \langle x^{(n-1)} \rangle (\langle x \rangle - n + 1), \quad (72)$$

where $x^{(n)} = x(x-1)\dots(x-n+1)$ is the falling factorial.

Let $a(x) := x^{(n-1)}$ and $b(x) := x - n + 1$ where $x \in \{0, 1, 2, \dots\}$. Note that both these functions are non-decreasing on the integers.

$$\begin{aligned} \langle a(x)b(x) \rangle - \langle a(x) \rangle \langle b(x) \rangle &= \sum_x a(x)b(x)P(x) - \sum_x a(x)P(x) \sum_y b(y)P(y), \\ &= \sum_{x,y} a(x)b(x)P(x)P(y) - \sum_x a(x)P(x) \sum_y b(y)P(y), \\ &= \sum_{x,y} a(x)(b(x) - b(y))P(x)P(y). \end{aligned} \quad (73)$$

Symmetrizing the last expression, we obtain

$$\begin{aligned} 2\langle a(x)b(x) \rangle - \langle a(x) \rangle \langle b(x) \rangle &= \sum_{x,y} a(x)(b(x) - b(y))P(x)P(y) + \sum_{x,y} a(y)(b(y) - b(x))P(x)P(y), \\ &= \sum_{x,y} (a(x) - a(y))(b(x) - b(y))P(x)P(y). \end{aligned} \quad (74)$$

Note that since both $a(x)$ and $b(x)$ are non-decreasing on the integers, it follows that if $x > y$ then $a(x) - a(y) \geq 0$ and $b(x) - b(y) \geq 0$, from which it follows that

$$\langle a(x)b(x) \rangle - \langle a(x) \rangle \langle b(x) \rangle \geq 0. \quad (75)$$

Since $x^{(n)} = a(x)b(x)$, the final result Eq. (72) is obtained.

Appendix B Generalization to cell-specific capture probabilities

Consider the general case of non-identical cells with an associated distribution of capture probabilities, $H(p_1, p_2, \dots, p_R)$, for R different molecular species. It then follows that Eq. (7) generalizes to

$$P(x_1, \dots, x_R) = \int_{\vec{p}} \sum_{y_1=0, \dots, y_R=0}^{\infty} P_{\text{bin}}^{p_1}(x_1|y_1) \dots P_{\text{bin}}^{p_R}(x_R|y_R) Q(y_1, \dots, y_R) H(p_1, \dots, p_R) dp_1 \dots dp_R, \quad (76)$$

where $Q(y_1, \dots, y_R)$ is the joint distribution of true counts and $P_{\text{bin}}^{p_i}(x_i|y_i)$ is the binomial distribution as defined in Eq. (2) with x replaced by x_i , y replaced by y_i and p by p_i .

Using Eq. (76), it is found that the generating function of the distribution of observed counts is given by

$$\begin{aligned} G(z_1, \dots, z_R, t) &= \int_{\vec{p}} \sum_{x_1=0}^{\infty} \dots \sum_{x_R=0}^{\infty} z_1^{x_1} \dots z_R^{x_R} P(x_1, \dots, x_R, t) H(p_1, \dots, p_R) dp_1 \dots dp_R \\ &= \int_{\vec{p}} \sum_{y_1=0}^{\infty} \dots \sum_{y_R=0}^{\infty} (1 - p_1(1 - z_1))^{y_1} \dots (1 - p_R(1 - z_R))^{y_R} Q(y_1, \dots, y_R, t) H(p_1, \dots, p_R) dp_1 \dots dp_R. \end{aligned} \quad (77)$$

By contrast, the generating function of the distribution of the true counts is given by

$$G(z_1, \dots, z_R, t)^* = \sum_{y_1=0}^{\infty} \dots \sum_{y_R=0}^{\infty} z_1^{y_1} \dots z_R^{y_R} Q(y_1, \dots, y_R, t). \quad (78)$$

Comparing the two generating functions, we see that the generating function of the distribution of observed counts can be obtained from the generating function of the distribution of the true counts by replacing z_i in the latter expression by $1 - p_i(1 - z_i)$ and then integrating over the distribution of the capture probabilities $H(p_1, \dots, p_R)$.

All results in Section 2 depend on the idea that technical noise amounts to a replacement of z_i in the latter expression by $1 - p_i(1 - z_i)$, and hence the main conclusions about renormalization of kinetic rates, under the influence of technical noise, remain the same, except that rate renormalization is now cell specific rather than the same for all cells. The same generalization can be shown to hold for the case of continuous protein concentrations observed using a Gaussian kernel.

Appendix C Hybrid Gillespie algorithm for PDMPs

In this appendix, we describe a hybrid Gillespie algorithm that extends the classical stochastic simulation algorithm (SSA) [65] to PDMPs for protein concentration dynamics. In contrast to the original SSA, which is formulated for reaction networks with discrete protein copy numbers, here the state variables are continuous protein concentrations. While the sampling of reaction times and reaction channels remains the same as in SSA, between these events the protein concentrations follow a deterministic ODE instead of a jump process of integer molecule counts. This hybrid algorithm has been used in simulations of stochastic gene expression [66, 67, 68], and here we apply it to simulate trajectories generated by the effective reaction set (64). In our framework, each protein species Y_i is governed by a PDMP: Y_i increases instantaneously at synthesis events (concentration bursts) and decays deterministically between them. We first provide the algorithm for the actual protein concentration and then describe the modifications required to simulate observed and mapped trajectories.

Suppose bursts in the system occur at time t_k , $k \in \mathbb{N}$. Bursts of protein Y_i occur according to an inhomogeneous Poisson process with rate $\alpha_i(\vec{y}(t), t)$. The burst size B_i is drawn from an exponential distribution with mean β_i and is generated as follows:

$$B_i = -\beta_i \ln(u), \quad u \sim U(0, 1), \quad (79)$$

where u is a pseudorandom number drawn from the uniform distribution on the interval $(0, 1)$. When a burst of the i th species occurs, the state of Y_i updates to $y_i(t_k^+) := y_i(t_k) + B_i$, while the concentrations of other species remain the same.

Between bursts, each protein species Y_i degrades deterministically according to the corresponding dynamical system $A_i(\vec{y}, t)$ (see Eq. (41) for details). In applications (Sections 3.3–3.5), we assume that $A_i(\vec{y}, t) = -\gamma_i(t)y_i(t)$ with the following solution:

$$y_i(t) = y_i(t_k^+) \exp\left\{-\int_{t_k}^t \gamma_i(z) dz\right\}, \quad t \in (t_k, t_{k+1}). \quad (80)$$

If the degradation rate is constant, $\gamma_i(t) \equiv \gamma_i$, then the protein concentration decays exponentially at rate γ_i .

The simulation process of the actual protein concentration is as follows. We initialize the process at time $t_0 = 0$ with a state \vec{y}_0 that can be either deterministic or sampled from the chosen initial distribution $Q_0(\vec{y})$. At the current event time t_k and state $\vec{y}(t_k)$ we evaluate instantaneous reaction propensities $\alpha_i = \alpha_i(\vec{y}(t_k), t_k)$. The candidate waiting times for the next event are sampled by the first reaction method as

$$\tau_i = -\frac{\ln u_i}{\alpha_i}, \quad u_i \sim U(0, 1).$$

The next reaction occurs at time $t + \tau^*$, $\tau^* = \min_i \tau_i$, with species $j = \arg \min_i \tau_i$. On the interval $(t_k, t_k + \tau^*)$ all species evolve deterministically as per Eq. (80). When the burst time is reached, apply the synthesis update on the selected species by drawing a burst size B_j from the exponential distribution with mean β_j , and update the state of the system accordingly. Repeat this procedure with $k \leftarrow k + 1$ until $t_{k+1} \geq T$; in this case, we calculate the deterministic decay on the interval (t_k, T) and stop. The pseudocode for this process is provided in Algorithm 1.

To simulate “true” observed trajectories of the protein concentration, we first generate the actual protein trajectory \vec{y} using Algorithm 1. For each recorded data point (concentration $y_i(t)$), we then model technical noise by drawing an observed value $x_i(t)$ from the Gaussian observation kernel (44) with the mean $p_i y_i(t)$ and variance

$p_i(1 - p_i)y_i(t)$, where p_i is the capture probability for species i . Each draw is independent across species and time points. There are two special cases that should be handled separately. If $p_i = 0$, then the protein cannot be observed and we set $x_i(t) = 0$. If $p_i = 1$, then the capture process is perfect and the observed trajectory coincides with the actual one; in this case, we set $x_i(t) = y_i(t)$.

To simulate the mapped trajectories, we replace the actual parameter values with the rescaled ones. In the applications described in Section 3.5, we find that the mean burst size β_i is mapped to $p_i\beta_i$, and the constants K_i are mapped to $K_i \prod_{j=1}^N p_j^{n_{ij}}$, where n_{ij} are Hill coefficients. After the rescaling, we run exactly the same hybrid Gillespie algorithm (Algorithm 1), but now we interpret the simulated data as mapped concentrations $\vec{x}(t)$. The special cases $p_i = 0$ and $p_i = 1$ are handled the same as in the workflow of observed trajectories. Thus, the mapped trajectories correspond to an effective PDMP that approximates the observed process.

Algorithm 1 Hybrid Gillespie (PDMP) for the effective system (64)

Require: terminal time T , initial state \vec{y}_0 or distribution $Q_0(\vec{y})$, system size N

Require: parameters: $\vec{K}, \vec{\beta}, \vec{\rho}_u, \vec{\rho}_b, \vec{\gamma}$, matrix of Hill coefficients n ; optional: K number of records in (t_k, t_{k+1})

Require: functions:

- ALPHA $_i(\vec{y}, t)$ – propensities $a_i = \alpha_i(\vec{y}, t)$ at time t ; given by Eq. (65)
- DECAY $(\vec{y}, t, \Delta t)$ – deterministic decay from state $\vec{y}(t)$ to $\vec{y}(t + \Delta t)$; given by (80)
- BURST (i) drawing B_i from exponential distribution with mean β_i ; given by Eq. (79)

```

1:  $t \leftarrow 0$ ,  $\vec{y} \leftarrow \vec{y}_0$  (or sample  $\vec{y} \sim Q_0$ ),  $k \leftarrow 0$ 
2: while  $t < T$  do
3:    $a_{1:N} \leftarrow \text{ALPHA}_{1:N}(\vec{y}, t)$  ▷ propensities at the current state and time
4:   for  $i = 1, \dots, N$  do
5:     draw  $u_i \sim \text{Unif}(0, 1)$ 
6:      $\tau_i \leftarrow \begin{cases} -\ln U_i / a_i, & a_i > 0 \\ +\infty, & a_i = 0 \end{cases}$ 
7:   end for
8:    $\tau^* \leftarrow \min_i \tau_i$ ,  $j \leftarrow \arg \min_i \tau_i$  ▷ first-reaction method
9:   if  $K > 0$  then
10:    for  $m = 0, \dots, K - 1$  do:
11:       $dt = m \cdot \tau^* / (K - 1)$  ▷  $K$  time points  $(t, t + dt, \dots, t_k + \tau^*)$ 
12:      record  $(t + dt, \text{DECAY}(\vec{y}, t, dt))$ 
13:    end for
14:  end if
15:  if  $t + \tau^* \geq T$  then ▷ final step
16:     $\vec{y} \leftarrow \text{DECAY}(\vec{y}, t, \Delta t = T - t)$ 
17:     $t \leftarrow T$ ; break
18:  end if
19:   $\vec{y} \leftarrow \text{DECAY}(\vec{y}, t, \tau^*)$ ,  $t \leftarrow t + \tau^*$ ,  $y_j \leftarrow y_j + \text{BURST}(j)$  ▷ update system state
20: end while
21: return trajectory  $(t, \vec{y})$  (or recorded snapshots)
```

References

- [1] M. Levine and E. H. Davidson, “Gene regulatory networks for development,” *Proceedings of the National Academy of Sciences*, 102, (14), 4936–4942, 2005.
- [2] E. H. Davidson, “Emerging properties of animal gene regulatory networks,” *Nature*, 468, (7326), 911–920, 2010.
- [3] E. H. Davidson and D. H. Erwin, “Gene regulatory networks and the evolution of animal body plans,” *Science*, 311, (5762), 796–800, 2006.
- [4] M. B. Elowitz, A. J. Levine, E. D. Siggia, and P. S. Swain, “Stochastic gene expression in a single cell,” *Science*, 297, (5584), 1183–1186, 2002.
- [5] H. De Jong, “Modeling and simulation of genetic regulatory systems: A literature review,” *Journal of computational biology*, 9, (1), 67–103, 2002.

- [6] M. Thattai and A. Van Oudenaarden, “Intrinsic noise in gene regulatory networks,” *Proceedings of the National Academy of Sciences*, 98, (15), 8614–8619, 2001.
- [7] M. Hegland, C. Burden, L. Santoso, S. MacNamara, and H. Booth, “A solver for the stochastic master equation applied to gene regulatory networks,” *Journal of computational and applied mathematics*, 205, (2), 708–724, 2007.
- [8] Z. Cao and R. Grima, “Linear mapping approximation of gene regulatory networks with stochastic dynamics,” *Nature communications*, 9, (1), 3305, 2018.
- [9] A. Ribeiro, R. Zhu, and S. A. Kauffman, “A general modeling strategy for gene regulatory networks with stochastic dynamics,” *Journal of computational Biology*, 13, (9), 1630–1639, 2006.
- [10] C. Jia and R. Grima, “Holimap: An accurate and efficient method for solving stochastic gene network dynamics,” *Nature Communications*, 15, (1), 6557, 2024.
- [11] R. Grima, D. R. Schmidt, and T. J. Newman, “Steady-state fluctuations of a genetic feedback loop: An exact solution,” *The Journal of chemical physics*, 137, (3), 2012.
- [12] N. Kumar, T. Platini, and R. V. Kulkarni, “Exact distributions for stochastic gene expression models with bursting and feedback,” *Physical review letters*, 113, (26), 268105, 2014.
- [13] F. Bocci, D. Jia, Q. Nie, M. K. Jolly, and J. Onuchic, “Theoretical and computational tools to model multistable gene regulatory networks,” *Reports on Progress in Physics*, 86, (10), 106601, 2023.
- [14] A. Gupta and M. Khammash, “Frequency spectra and the color of cellular noise,” *Nature communications*, 13, (1), 4305, 2022.
- [15] P. V. Kharchenko, L. Silberstein, and D. T. Scadden, “Bayesian approach to single-cell differential expression analysis,” *Nature methods*, 11, (7), 740–742, 2014.
- [16] R. Lopez, J. Regier, M. B. Cole, M. I. Jordan, and N. Yosef, “Deep generative modeling for single-cell transcriptomics,” *Nature methods*, 15, (12), 1053–1058, 2018.
- [17] G. Eraslan, L. M. Simon, M. Mircea, N. S. Mueller, and F. J. Theis, “Single-cell rna-seq denoising using a deep count autoencoder,” *Nature communications*, 10, (1), 390, 2019.
- [18] R. Jiang, T. Sun, D. Song, and J. J. Li, “Statistics or biology: The zero-inflation controversy about scRNA-seq data,” *Genome Biology*, 23, (1), 31, 2022.
- [19] C. Jia, “Kinetic foundation of the zero-inflated negative binomial model for single-cell rna sequencing data,” *SIAM Journal on Applied Mathematics*, 80, (3), 1336–1355, 2020.
- [20] A. M. Klein, L. Mazutis, I. Akartuna, N. Tallapragada, A. Veres, V. Li, L. Peshkin, D. A. Weitz, and M. W. Kirschner, “Droplet barcoding for single-cell transcriptomics applied to embryonic stem cells,” *Cell*, 161, (5), 1187–1201, 2015.
- [21] W. Tang, F. Bertaux, P. Thomas, C. Stefanelli, M. Saint, S. Marguerat, and V. Shahrezaei, “Baynorm: Bayesian gene expression recovery, imputation and normalization for single-cell RNA-sequencing data,” *Bioinformatics*, 36, (4), 1174–1181, 2020.
- [22] C. Ziegenhain, B. Vieth, S. Parekh, B. Reinus, A. Guillaumet-Adkins, M. Smets, H. Leonhardt, H. Heyn, I. Hellmann, and W. Enard, “Comparative analysis of single-cell RNA sequencing methods,” *Molecular Cell*, 65, (4), 631–643, 2017.
- [23] D. Grün, L. Kester, and A. Van Oudenaarden, “Validation of noise models for single-cell transcriptomics,” *Nature Methods*, 11, (6), 637–640, 2014.
- [24] R. Salomon, D. Kaczorowski, F. Valdes-Mora, R. E. Nordon, A. Neild, N. Farbehi, N. Bartonicek, and D. Gallego-Ortega, “Droplet-based single cell RNAseq tools: A practical guide,” *Lab on a Chip*, 19, (10), 1706–1727, 2019.
- [25] 10x Genomics, *What fraction of mRNA transcripts are captured per cell?* <https://kb.10xgenomics.com/hc/en-us/articles/360001539051-What-fraction-of-mRNA-transcripts-are-captured-per-cell>, Accessed: December 1, 2025, 10x Genomics Knowledge Base, 2025.
- [26] H. Specht, E. Emmott, A. A. Petelski, R. G. Huffman, D. H. Perlman, M. Serra, P. Kharchenko, A. Koller, and N. Slavov, “Single-cell proteomic and transcriptomic analysis of macrophage heterogeneity using scope2,” *Genome biology*, 22, (1), 50, 2021.
- [27] A. Leduc, R. G. Huffman, J. Cantlon, S. Khan, and N. Slavov, “Exploring functional protein covariation across single cells using npop,” *Genome Biology*, 23, (1), 261, 2022.
- [28] C. Vanderaa and L. Gatto, “Revisiting the thorny issue of missing values in single-cell proteomics,” *Journal of Proteome Research*, 22, (9), 2775–2784, 2023.
- [29] W. Tang, A. C. S. Jørgensen, S. Marguerat, P. Thomas, and V. Shahrezaei, “Modelling capture efficiency of single-cell rna-sequencing data improves inference of transcriptome-wide burst kinetics,” *Bioinformatics*, 39, (7), btad395, 2023.
- [30] A. Sukys and R. Grima, “Cell-cycle dependence of bursty gene expression: Insights from fitting mechanistic models to single-cell RNA-seq data,” *Nucleic Acids Research*, 53, (7), gkaf295, 2025.

- [31] P. Trzaskoma, S. Jung, A. Pękowska, C. H. Bohrer, X. Wang, F. Naz, S. Dell’Orso, W. D. Dubois, A. Olivera, S. V. Vartak, et al., “3d chromatin architecture, brd4, and mediator have distinct roles in regulating genome-wide transcriptional bursting and gene network,” *Science Advances*, 10, (32), eadl4893, 2024.
- [32] Y. Wang, Z. Shu, Z. Cao, and R. Grima, “From noise to models to numbers: Evaluating negative binomial models and parameter estimations in single-cell rna-seq,” *bioRxiv*, 2025–05, 2025.
- [33] J. Peccoud and B. Ycart, “Markovian modeling of gene-product synthesis,” *Theoretical population biology*, 48, (2), 222–234, 1995.
- [34] A. Raj, C. S. Peskin, D. Tranchina, D. Y. Vargas, and S. Tyagi, “Stochastic mrna synthesis in mammalian cells,” *PLoS biology*, 4, (10), e309, 2006.
- [35] J. Szavits-Nossan and R. Grima, “Steady-state distributions of nascent rna for general initiation mechanisms,” *Physical Review Research*, 5, (1), 013064, 2023.
- [36] S. Braichenko, J. Holehouse, and R. Grima, “Distinguishing between models of mammalian gene expression: Telegraph-like models versus mechanistic models,” *Journal of the Royal Society Interface*, 18, (183), 20210510, 2021.
- [37] Z. Cao, T. Filatova, D. A. Oyarzún, and R. Grima, “A stochastic model of gene expression with polymerase recruitment and pause release,” *Biophysical Journal*, 119, (5), 1002–1014, 2020.
- [38] R. Karmakar and A. K. Das, “Effect of transcription reinitiation in stochastic gene expression,” *Journal of Statistical Mechanics: Theory and Experiment*, 2021, (3), 033502, 2021.
- [39] T. Zhou and J. Zhang, “Analytical results for a multistate gene model,” *SIAM Journal on Applied Mathematics*, 72, (3), 789–818, 2012.
- [40] F. Jiao, J. Li, T. Liu, Y. Zhu, W. Che, L. Bleris, and C. Jia, “What can we learn when fitting a simple telegraph model to a complex gene expression model?” *PLOS Computational Biology*, 20, (5), e1012118, 2024.
- [41] L. Ham, D. Schnoerr, R. D. Brackston, and M. P. Stumpf, “Exactly solvable models of stochastic gene expression,” *The Journal of Chemical Physics*, 152, (14), 2020.
- [42] U. Herbach, “Stochastic gene expression with a multistate promoter: Breaking down exact distributions,” *SIAM Journal on Applied Mathematics*, 79, (3), 1007–1029, 2019.
- [43] A. Klindziuk and A. B. Kolomeisky, “Theoretical investigation of transcriptional bursting: A multistate approach,” *The Journal of Physical Chemistry B*, 122, (50), 11969–11977, 2018.
- [44] C. R. Bartman, N. Hamagami, C. A. Keller, B. Giardine, R. C. Hardison, G. A. Blobel, and A. Raj, “Transcriptional burst initiation and polymerase pause release are key control points of transcriptional regulation,” *Molecular cell*, 73, (3), 519–532, 2019.
- [45] K. Adelman and J. T. Lis, “Promoter-proximal pausing of rna polymerase ii: Emerging roles in metazoans,” *Nature Reviews Genetics*, 13, (10), 720–731, 2012.
- [46] W. Shao and J. Zeitlinger, “Paused rna polymerase ii inhibits new transcriptional initiation,” *Nature genetics*, 49, (7), 1045–1051, 2017.
- [47] Z. Cao and R. Grima, “Analytical distributions for detailed models of stochastic gene expression in eukaryotic cells,” *Proceedings of the National Academy of Sciences*, 117, (9), 4682–4692, 2020.
- [48] A. Singh and P. Bokes, “Consequences of mrna transport on stochastic variability in protein levels,” *Biophysical journal*, 103, (5), 1087–1096, 2012.
- [49] V. Shahrezaei and P. S. Swain, “Analytical distributions for stochastic gene expression,” *Proceedings of the National Academy of Sciences*, 105, (45), 17256–17261, 2008.
- [50] I. Golding, J. Paulsson, S. M. Zawilski, and E. C. Cox, “Real-time kinetics of gene activity in individual bacteria,” *Cell*, 123, (6), 1025–1036, 2005.
- [51] G.-W. Li and X. S. Xie, “Central dogma at the single-molecule level in living cells,” *Nature*, 475, (7356), 308–315, 2011.
- [52] N. Rosenfeld, M. B. Elowitz, and U. Alon, “Negative autoregulation speeds the response times of transcription networks,” *Journal of molecular biology*, 323, (5), 785–793, 2002.
- [53] S. S. Shen-Orr, R. Milo, S. Mangan, and U. Alon, “Network motifs in the transcriptional regulation network of escherichia coli,” *Nature genetics*, 31, (1), 64–68, 2002.
- [54] J. Holehouse, Z. Cao, and R. Grima, “Stochastic modeling of autoregulatory genetic feedback loops: A review and comparative study,” *Biophysical Journal*, 118, (7), 1517–1525, 2020.
- [55] G. C. Innocentini, A. F. Ramos, and J. E. M. Hornos, “Comment on “steady-state fluctuations of a genetic feedback loop: An exact solution”[j. chem. phys. 137, 035104 (2012)],” *The Journal of chemical physics*, 142, (2), 2015.
- [56] P. Thomas, N. Popović, and R. Grima, “Phenotypic switching in gene regulatory networks,” *Proceedings of the National Academy of Sciences*, 111, (19), 6994–6999, 2014.

- [57] H. Qian, P.-Z. Shi, and J. Xing, “Stochastic bifurcation, slow fluctuations, and bistability as an origin of biochemical complexity,” *Physical Chemistry Chemical Physics*, 11, (24), 4861–4870, 2009.
- [58] N. Friedman, L. Cai, and X. S. Xie, “Linking stochastic dynamics to population distribution: An analytical framework of gene expression,” *Physical review letters*, 97, (16), 168302, 2006.
- [59] S. Zeiser, U. Franz, and V. Liebscher, “Autocatalytic genetic networks modeled by piecewise-deterministic markov processes,” *Journal of mathematical biology*, 60, (2), 207–246, 2010.
- [60] M. C. Mackey, M. Tyran-Kaminska, and R. Yvinec, “Dynamic behavior of stochastic gene expression models in the presence of bursting,” *SIAM Journal on Applied Mathematics*, 73, (5), 1830–1852, 2013.
- [61] E. T. Copson and E. T. Copson, *Asymptotic expansions*. Cambridge university press, 2004.
- [62] Y. Taniguchi, P. J. Choi, G.-W. Li, H. Chen, M. Babu, J. Hearn, A. Emili, and X. S. Xie, “Quantifying e. coli proteome and transcriptome with single-molecule sensitivity in single cells,” *science*, 329, (5991), 533–538, 2010.
- [63] T. S. Gardner, C. R. Cantor, and J. J. Collins, “Construction of a genetic toggle switch in escherichia coli,” *Nature*, 403, (6767), 339–342, 2000.
- [64] M. B. Elowitz and S. Leibler, “A synthetic oscillatory network of transcriptional regulators,” *Nature*, 403, (6767), 335–338, 2000.
- [65] D. T. Gillespie, “Exact stochastic simulation of coupled chemical reactions,” *The journal of physical chemistry*, 81, (25), 2340–2361, 1977.
- [66] P. Bokes, J. R. King, A. T. Wood, and M. Loose, “Transcriptional bursting diversifies the behaviour of a toggle switch: Hybrid simulation of stochastic gene expression,” *Bulletin of mathematical biology*, 75, (2), 351–371, 2013.
- [67] A. Duncan, R. Erban, and K. Zygalakis, “Hybrid framework for the simulation of stochastic chemical kinetics,” *Journal of Computational Physics*, 326, 398–419, 2016.
- [68] I. Zabaikina and P. Bokes, “Maintenance of steady-state mrna levels by a microrna-based feed forward loop in the presence of stochastic gene expression noise,” *European Journal of Applied Mathematics*, 36, (1), 143–160, 2025.